

Continuum Dark Matter

Csaba Csáki,^a Sungwoo Hong,^{a,b,c} Gowri Kurup,^{a,d} Seung J. Lee,^e Maxim Perelstein,^a and Wei Xue^f

^a*Department of Physics, LEPP, Cornell University, Ithaca, NY 14853, USA*

^b*Department of Physics, The University of Chicago, Chicago, IL 60637, USA*

^c*Argonne National Laboratory, Lemont, IL 60439, USA*

^d*Rudolf Peierls Centre for Theoretical Physics, University of Oxford, Parks Rd, Oxford OX1 3PJ, United Kingdom*

^e*Department of Physics, Korea University, Seoul, 136-713, Korea*

^f*Department of Physics, University of Florida, Gainesville, FL 32611, USA*

ABSTRACT: We initiate the study of dark matter models based on a gapped continuum. Dark matter consists of a mixture of states with a continuous mass distribution, which evolves as the universe expands. We present an effective field theory describing the gapped continuum, outline the structure of the Hilbert space and show how to deal with the thermodynamics of such a system. This formalism enables us to study the cosmological evolution and phenomenology of gapped continuum DM in detail. As a concrete example, we consider a weakly-interacting continuum (WIC) model, a gapped continuum counterpart of the familiar WIMP. The DM interacts with the SM via a Z-portal. The model successfully reproduces the observed relic density, while direct detection constraints are avoided due to the effect of continuum kinematics. The model has unique observational consequences, including continuous decays of DM states throughout cosmological history, as well as cascade decays of DM states produced at colliders. We also describe how the WIC theory can arise from a local, unitary scalar QFT propagating on a five-dimensional warped background with a soft wall.

Contents

1	Introduction	2
2	Preview of Continuum Effects in DM Phenomenology	5
3	Physics of Gapped Continuum	8
3.1	Free Continuum QFT with a Gap	9
3.2	Equilibrium Thermodynamics	11
3.3	Non-equilibrium Thermodynamics	13
4	Freeze-Out of Continuum Dark Matter	14
4.1	Boltzmann Equation for Continuum Freeze-Out	14
4.2	Freeze-Out in a Toy Model	15
5	WIC model using the Vector Boson Portal	17
5.1	4D Effective Z -portal Model	17
5.2	Relic abundance of continuum Z -portal DM	19
6	Continuum Spectral Density and UV-Complete WIC Model from a Warped Spacetime	22
6.1	The Cabrer-von Gersdorff-Quiros (CGQ) Background	22
6.2	Realistic Gapped Continuum Spectral Density	24
6.3	5D Z -portal Model	28
7	Conclusion and Outlook	29
A	Gapped Continuum from Five-Dimensional Flat Space	30
A.1	Infinite 5D and Spectral Density	31
A.2	Compactified Theory and KK Picture	31
A.3	Hilbert Space, Orthonormality and Completeness	32
A.4	Boltzmann Equation	33
B	Spectral Density Near the Gap	34
C	AdS/CFT Duality of Gapped Continuum	36

1 Introduction

The microscopic nature of dark matter (DM) remains one of the most important outstanding questions in fundamental physics [1]. DM cannot consist of any of the Standard Model (SM) particles, providing firm evidence for new physics. Many models have been proposed by theorists, covering a mass range between 10^{-22} to 10^{67} eV, as well as various interaction portals to the SM [2–4]. Extensive experimental efforts are underway aiming to either detect non-gravitational signatures of ambient DM, or to produce DM particles in the lab [5–7]. Both approaches can yield powerful hints to illuminate the nature of DM; however, so far, neither has been successful in detecting signals of DM. In fact so far we don’t even know for sure whether DM consists of an elementary particle, composite bound states [8, 9], extended objects such as Q-balls [10], or even macroscopic entities such as primordial black holes [11–13] and ultra-compact mini-halos [14–18]. It is therefore timely to explore the spectrum of theoretical possibilities for DM, as such explorations are both important in their own right and can provide guidance essential for future experimental searches.

In this paper, we propose a new conceptual framework in which dark matter is described by a *gapped continuum*, rather than an ordinary particle. In quantum field theories (QFTs) with a gapped continuum, the singly-excited states are characterized by a continuous parameter μ^2 , in addition to the usual 3-momentum \mathbf{p} . The parameter μ^2 plays the role of mass in the kinematic relation $p^2 = \mu^2$ for each state. The number of states is proportional to $\int \rho(\mu^2) d\mu^2$, where ρ is the *spectral density* of the theory, conventionally defined in QFT’s as

$$\langle 0 | \Phi(p) \Phi(-p) | 0 \rangle = \int \frac{d\mu^2}{2\pi} \frac{i\rho(\mu^2)}{p^2 - \mu^2 + i\epsilon} . \quad (1.1)$$

The word “gapped” refers to continuum QFTs in which the function ρ has no support below some finite *gap scale*, μ_0^2 . For application to DM physics we will not be concerned with the exact origin of the continuum. We will simply assume that some form of dynamics created such a continuum as its effective description, and will treat it as a “free continuum”, as discussed in detail in section 3. Later in section 6 we will provide one possible origin of such a continuum by considering a warped extra dimensional soft wall background.

We will construct DM models based on continuum QFT with the gap around the electroweak scale, $\mu_0 \sim 100$ GeV, and including interactions to the electroweak (EW) sector of the SM. We will call the resulting type of model the Weakly Interacting Continuum (WIC) DM model. A typical spectral density for the class of theories we consider is shown in fig. 1.

The key feature of WIC models is that DM cannot be thought of as a gas of particles of the same mass, or even as a mixture of gases of a finite number of DM species with different masses.¹ Instead, in cosmology DM states follow a continuous mass distribution determined by the product of spectral density and occupation number. In the expanding universe, this distribution is time-dependent (and can in principle depend on spatial location as well),

¹In particular, continuum DM is very different from dynamical DM models proposed in [19, 20], both in its theoretical framework and phenomenological signatures. In [21, 22], a continuum is used as the mediator to the dark sector, while here the continuum is the dark sector itself.

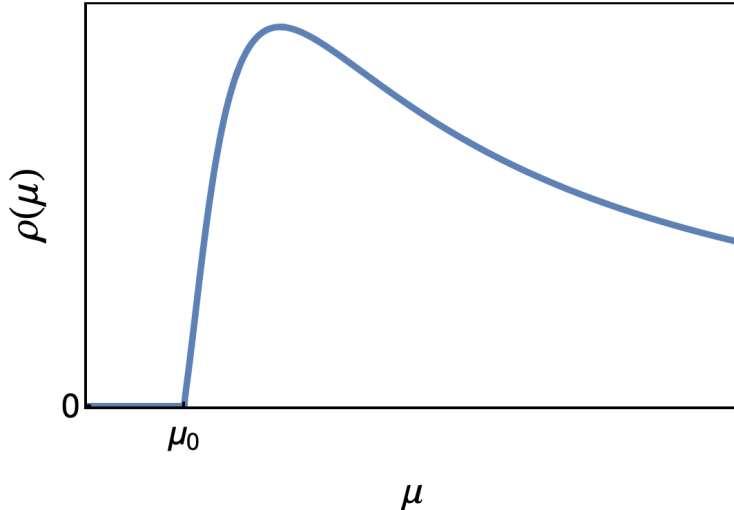


Figure 1. A typical shape of the spectral density $\rho(\mu)$ with gap scale μ_0 .

and its evolution is governed by generalized Boltzmann equations that we will discuss. In our model, the distribution of the DM mass today is clustered in a narrow window slightly above the gap scale, but in the early universe it was much more broadly distributed.

Continuum DM has striking phenomenological consequences. For example, while the DM state at the very bottom of the spectrum can be stable, *e.g.* due to a discrete symmetry, any other state in the continuum must be unstable with respect to decaying into lighter DM states. The continuum DM gas exists in a state of permanent decay. This leads to distinctive cosmological signatures and bounds. In particular, it is possible that DM decays can re-ionize the universe during the “dark ages”, and cosmic microwave background (CMB) observations place an important bound on the model. Another striking feature is the absence of elastic scattering of DM on an SM particle such as a nucleon or an electron: in a continuum theory, any such scattering induces a change in the DM state’s mass, and is therefore inelastic. A non-relativistic DM state with mass near the gap scale can only scatter into a narrow band of the continuum states due to kinematic constraints. Because of this, direct detection rates for continuum DM are strongly suppressed with respect to a comparable single-particle DM model. This will allow us to build a model in which DM communicates with the SM via a Z -portal, has thermal relic density, but is nevertheless not ruled out by direct detection experiments [23–26]. Colliders, on the other hand, can provide a unique, smoking-gun signature of continuum DM: a typical DM state produced in a collider would undergo multiple decays into progressively lighter DM states within the detector, with softer SM energy deposits at each step and a collider-stable DM state at the end of the cascade appearing as missing energy.

We emphasize that many predictions of the continuum DM model, including thermal freeze-out (relic density), late decays (reionization and CMB), annihilation in the DM halos (indirect detection), and scattering with target nuclei or electrons (direct detection), are

governed by the shape of the spectral density very close to the gap scale μ_0 . Remarkably, for a broad class of gapped continuum QFT's, $\rho(\mu)$ near the gap scale takes a universal shape of the form $\rho(\mu) \propto \sqrt{\mu^2/\mu_0^2 - 1}$. We show this in section 6 and appendix B. This feature makes the continuum DM physics highly model independent. On the other hand, colliders can play a complementary role in uncovering the full picture of the continuum sector.

The appearance of a continuum is very common in QFT's. The spectrum of conformal field theories (CFTs) necessarily forms a continuum since the theory does not admit any mass scales. Georgi's unparticles [27, 28] also describe a continuum, and have been widely used for various particle physics applications. While continuum with a mass gap has been less commonly used, one can still find many examples of a gapped continuum both in particle and condensed matter physics. In string theory such a gapped continuum shows up when one has a large number of D3 branes distributed on a disc (which is dual to $\mathcal{N} = 4$ SUSY broken to $\mathcal{N} = 2$ via masses for two chiral adjoints, for a related large literature see [29–31]). In particle physics the simplest example of a gapped continuum was proposed by Cabrer, von Gersdorff and Quiros (CGQ) [32], based on a warped extra dimension, which is the construction we will also be relying on most in this paper. Gapped continuum has been applied to both Higgs physics (“quantum critical Higgs” where the particle-like Higgs is mixed with a continuum [33]) and for an alternative solution of the hierarchy problem (“continuum top partners” [34] see also [35, 36]). A gapped continuum also readily shows up in condensed matter physics, for example the edge modes in the quantum Hall effect, or the spectral density around a quantum critical point [37, 38]. There are also well-known examples in $d < 4$ dimensions such as 2d Ising model [39, 40], 2d $SU(N)$ Yang-Mills theory in large- N limit [41], and 2d $SU(2)$ Thirring model [42].

The paper is organized as follows. We start with a preview of the novel phenomenological signatures that are unique to continuum dark matter in section 2. We then describe the theoretical formalism that allows us to derive physical predictions from gapped continuum QFT's, both at zero temperature and in thermodynamics. This is the subject of section 3. In section 4, we specialize to DM physics and derive the Boltzmann equation (BE) for continuum DM freeze-out. In order to demonstrate the use of our formalism, we study the freeze-out of scalar continuum DM in a simple toy model. Next, in section 5, we present the fully realistic continuum Z -portal model and use it to calculate the relic abundance of DM. Figure 3 illustrates the parameter space that can reproduce the observed relic density as well as satisfy all relevant experimental constraints. (The detailed discussion of phenomenology of the Z -portal continuum DM is contained in the companion paper [43].) In section 6, we provide a more complete description of the continuum Z -portal, based on a theory in warped five-dimensional spacetime (soft-wall background). Finally, we present our conclusion and outlook in section 7. Some of important topics are presented in the form of appendices. In appendix A, we study a scalar field in a flat 5D and show that its 4D spectrum can be interpreted as a gapped continuum. This exercise yields interesting insights about the interpretation of spectral density, the Hilbert space of gapped continuum theories, and their thermodynamics. In appendix B, we provide a general proof for the properties of the spectral density near the gap scale. Finally in appendix C, we describe the

4D dual description of our 5D warped model. We obtain the CFT dual picture in terms of canonically normalized composite continuum modes, which mix with external/elementary fields. We show that once we resum these mixings, rates computed using the standard 4D formulae reproduce the equations introduced in section 3.

2 Preview of Continuum Effects in DM Phenomenology

Before presenting a systematic discussion of the physics of a gapped continuum, this section gives a preview of the novel aspects of continuum physics that will distinguish it from ordinary particle-based DM models.

Late decay

One of the important distinguishing features of continuum DM are the decays

$$\text{DM}(\mu_1) \rightarrow \text{DM}(\mu_2) + \text{SM}, \quad (2.1)$$

where $\text{DM}(\mu)$ refers to a dark matter state of mass μ , while “SM” denotes one or more SM particles. Since all continuum states carry the same quantum numbers (including any stabilizing symmetry that prevents DM decays to fully SM final states), such decays will necessarily occur continuously throughout the history of the universe. This is in sharp contrast with particle DM models, where there is at most a handful of long-lived states decaying at specific epochs determined by their intrinsic decay widths.

In the early universe, DM is in thermal and chemical equilibrium with the SM, and the mass distribution of the DM states is determined by the product of spectral density and the Boltzmann factor (for details, see section 3.2). As the temperature drops below the gap scale μ_0 , the DM decouples from the SM and the total number of DM states is frozen out, just like for the usual thermal-relic particle DM. However, the mass distribution of the DM states continues to evolve, thanks to decays (2.1). The decays shift the distribution towards lower masses, closer to the gap scale. Lifetime of a DM state $\Gamma^{-1}(\mu)$ increases with decreasing mass, due to both phase-space suppression and the fact that there are fewer states for it to decay into. Schematically,

$$\Gamma(\mu) \sim g^2 \Delta^p \mu_0^{1-p}, \quad (2.2)$$

where g is the strength of DM-SM coupling, p is a model-dependent positive number, and $\Delta = \mu - \mu_0$. If $t_0 \sim H^{-1}$ is the age of the universe, only DM states for which $\Gamma \lesssim H$ can still be present. This condition can be used to find the typical mass of the DM states at any given time. For example, in the model considered in detail in this paper, the DM states are currently clustered within a few hundred keV above the gap scale. It also indicates that on average, each DM state undergoes roughly one decay per Hubble time, or in other words an order-one fraction of DM states will decay during each doubling of the scale factor.

The continuous DM decays also lead to potentially observable effects in cosmology. If the SM particles produced in the decay interact electromagnetically (*i.e.* all SM particles except neutrinos), the decays that occur after CMB decoupling can reionize hydrogen,

drastically changing the optical depth for CMB photons [44–47]. This places a stringent bound on the structure of the continuum DM models. In the Z-portal model considered in this paper, the bound can be satisfied only if the DM decays to electron-positron pairs are kinematically forbidden, $\Delta \lesssim \text{MeV}$, at and after the CMB decoupling time. This condition implies a *lower* bound on the strength of the DM coupling to SM, see fig. 3.

Direct detection

A very important and generic feature of gapped continuum DM is the suppression of direct detection rates. The scattering process relevant for direct detection is

$$\text{DM}(\mu_1) + \text{SM} \rightarrow \text{DM}(\mu_2) + \text{SM}. \quad (2.3)$$

The cross section can be schematically written as

$$\sigma \sim \int \frac{d\mu_2^2}{2\pi} \rho(\mu_2^2) \hat{\sigma}(\mu_1, \mu_2), \quad (2.4)$$

where $\hat{\sigma}$ is an ordinary particle $2 \rightarrow 2$ cross section, with the masses for the external particles replaced by the continuum parameters μ_1 and μ_2 . If the incoming DM state has mass $\mu_1 = \mu_0 + \Delta$, the range of kinematically accessible values of μ_2 is $[\mu_0, \mu_0 + \Delta + Q]$, where Q is the kinetic energy of the collision in the center-of-mass frame. As we argued above, continuous DM decays generically result in $\Delta \ll \mu_0$ in today’s universe, while $Q \ll \mu_0$ as long as ambient DM is non-relativistic. We can then estimate

$$\sigma_{\text{cont}} \sim \left(\frac{\Delta + Q}{\mu_0} \right)^{1+r} \sigma_{\text{particle}}, \quad (2.5)$$

where r is a positive number that depends on the behavior of the spectral density near the gap. (It will be shown in section 6 and appendix B that $r = 1/2$ in a broad class of warped-space 5D models of gapped continuum.) For example, in the specific model that will be considered in detail in this paper, continuous DM decays result in $\Delta \sim 100 \text{ keV}$ at the present time, while $Q \sim 1 \text{ keV}$ in the case of ambient weak-scale DM colliding with a nucleus. With μ_0 at the weak scale, this mechanism gives a spectacular suppression of the direct detection cross section by several orders of magnitude compared to a particle model with the same mass scale and interaction strength. We emphasize that this effect is entirely due to the continuous nature of the DM spectrum: intuitively, the suppression arises because only a tiny fraction of the DM spectrum is kinematically accessible in the scattering process (2.3) in a direct detection experiment.

In contrast, indirect detection relies on annihilation processes of the form $\text{DM}(\mu_1) + \text{DM}(\mu_2) \rightarrow \text{SM}_1 + \text{SM}_2$. Since there is no continuum state in the final state, the rates of these processes are unsuppressed. In fact, since $\mu_1 \approx \mu_2 \approx \mu_0$ in the current universe, both rates and kinematics of annihilation in the galactic halos are virtually identical for continuum and particle DM.

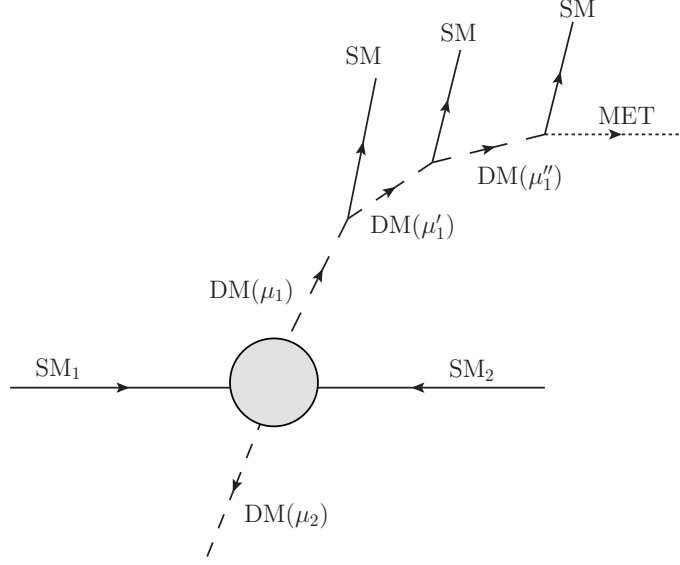


Figure 2. Schematic representation of collider signature of the continuum DM.

Colliders

Continuum DM states can be produced in colliders via

$$\text{SM}_1 + \text{SM}_2 \rightarrow \text{DM}(\mu_1) + \text{DM}(\mu_2). \quad (2.6)$$

All kinematically accessible DM modes will generically be produced. The total production cross section is schematically

$$\sigma \sim \int \frac{d\mu_1^2}{2\pi} \rho(\mu_1^2) \int \frac{d\mu_2^2}{2\pi} \rho(\mu_2^2) \hat{\sigma}(\mu_1, \mu_2). \quad (2.7)$$

If the collision energy is close to the threshold, the continuum kinematics leads to suppressed rates, similar to the case of direct detection. This effect may weaken collider bounds on the model. On the other hand, if collision energy is above the gap scale by an order-one factor, there is no kinematic suppression factor as in the case of direct detection, and the collider cross section is of the same order for continuum and particle DM. However, unlike particle DM, the continuum DM states quickly decay, see eq. (2.1). In fact, each state undergoes a series of decays, illustrated in fig. 2. Each decay produces SM particles (with progressively smaller energies at each step of the cascade) in addition to a DM state (with mass closer to the gap scale at each step of the cascade). Many such decays will occur within the detector, resulting in a high-multiplicity observable SM final state with characteristic pattern of energy distributions, in addition to missing energy due to the escaping long-lived DM states. A detailed study of this exciting and novel collider phenomenology will be pursued in future work.

3 Physics of Gapped Continuum

It is often stated that CFT's and theories with continuum spectra do not have a particle interpretation and no S-matrix can be defined. The main reason behind this is that the interactions leading to a non-trivial fixed point are also essential for producing the continuum spectrum of the theory. If one turns off the interactions, the spectrum changes from continuum into that of an ordinary free particle, hence the asymptotic states defined in the usual manner would not capture the physics of the system properly. This however does not imply that there would be anything wrong with these theories, nor that they could not be successfully used in particle physics for BSM sectors, but rather that one needs to find an alternative approach for defining scattering processes. Instead of relying on the definition of asymptotic states obtained by turning off the interactions, we will assume that the effects of the strong interactions can be captured by the fact that there is a non-trivial continuum (with a mass gap), and described by a (potentially non-local) effective Lagrangian

$$S = \int \frac{d^4 p}{(2\pi)^4} \Phi^\dagger(p) \Sigma(p^2) \Phi(p) \quad (3.1)$$

which is designed to properly reproduce the two-point function of theory

$$\int d^4 x e^{ip(x-y)} \langle 0 | T \Phi(x) \Phi^\dagger(y) | 0 \rangle = \langle 0 | \Phi(p) \Phi^\dagger(-p) | 0 \rangle = \frac{i}{\Sigma(p^2)} = \int \frac{d\mu^2}{2\pi} \frac{i \rho(\mu^2)}{p^2 - \mu^2 + i\epsilon}, \quad (3.2)$$

where $\rho(\mu^2)$ is the spectral density. We will assume that the effective description in eq. (3.1) is weakly coupled, hence Φ corresponding to a “generalized free field” [48]². Essentially we are assuming that the resulting continuum is free, hence we will refer to this scenario as a “free continuum theory”. In addition we perturb around generalized free continuum by introducing additional weak couplings to Φ and assume that the underlying structure described by the spectral density remains unchanged, resulting in a weakly interacting continuum. This picture will be supported by the concrete extra dimensional construction that we introduce in section 6. Φ will be the boundary value of a bulk scalar field propagating in a non-trivial “soft-wall”-type background, which itself is supposed to be the 5D dual of a strongly interacting 4D CFT-like theory (see appendix C for details). Σ will be the brane-to-brane propagator which can be calculated for a fixed background, and we will be adding interactions of Φ with SM fields assumed to be localized on the brane.

For a given Σ the spectral density ρ can be obtained as

$$\rho(p^2) = -2 \operatorname{Im} \frac{1}{\Sigma(p^2)}. \quad (3.3)$$

If $\Sigma(p^2) = (p^2 - m^2 + i\epsilon)$, this theory merely describes a free scalar *particle* with mass m^2 , corresponding to $\rho(\mu^2) \propto \delta(\mu^2 - m^2)$. When $\rho(\mu^2)$ has a non-vanishing support on continuum domain in μ^2 , the theory describes a continuum. In particular, if the spectral density has a continuous distribution starting at $\mu^2 \geq \mu_0^2 > 0$, we have a theory of gapped

²For more recent discussions on generalized free fields, see, for example, [49] and references therein.

continuum, with gap scale μ_0 . Note that a continuum contribution is always present even in the case of ordinary particles when one is considering the (loop-induced) multi-particle contributions to the spectral density. In the free continuum theories we are considering there is no one-particle pole and instead we have “tree-level” continuum present in $\rho(\mu^2)$, which represents the intrinsic continuum states. The best way to think of the continuum states is to view them as smeared out particles with a density of states: a finite physical effect is obtained only as collective effect after integrating over a finite energy interval weighted by the density of states. This density of states will be identified with the spectral density $\rho(\mu^2)$. Below we will systematically build up the formalism needed to most efficiently deal with such weakly coupled continuum states originating from a generalized free field, and present the formulae that are analog of those in ordinary particle physics. We will show that in spite of the inherent differences one can find a simple modification of the Hilbert-space construction for the free continuum that closely parallels that of ordinary particles, which will make the calculation of reaction rates quite straightforward.

An interaction between the gapped continuum and SM fields can be introduced in a standard QFT way: just use the corresponding field $\Phi(x)$ to build a local (gauge invariant) interaction term. For example, the “Higgs-portal” interaction will be

$$S_{\text{int}} = \int d^4x \lambda H^\dagger H(x) \Phi^\dagger \Phi(x) \quad (3.4)$$

where H is the SM Higgs doublet, and Φ is the operator responsible for the gapped continuum. While this simple interaction turns out to not lead to a phenomenologically viable DM model, we will use it as a toy model to illustrate the formalism, before presenting the fully realistic model in section 5 and section 6.

3.1 Free Continuum QFT with a Gap

Next we will present the basic construction of a free continuum. A pedagogical introduction to these states can also be found in appendix A where we show how the Kaluza-Klein (KK) states in a simple flat extra dimension can be interpreted as a continuum in 4D, which will also clarify what the right completeness and orthonormality conditions should be. A quick read of appendix A is highly recommended before moving on here.

We will start with the description of the Hilbert space. The single-mode sector will contain (in addition to ordinary 1-particle states corresponding to the SM) additional states labeled by $|\mathbf{p}, \mu^2\rangle$, which are eigenstates of Hamiltonian \hat{H} and 3-momentum $\hat{\mathbf{P}}$ such that

$$\begin{aligned} \hat{\mathbf{P}} |\mathbf{p}, \mu^2\rangle &= \mathbf{p} |\mathbf{p}, \mu^2\rangle, \\ \hat{H} |\mathbf{p}, \mu^2\rangle &= E_\mu |\mathbf{p}, \mu^2\rangle, \quad E_\mu \equiv \sqrt{\mathbf{p}^2 + \mu^2}. \end{aligned} \quad (3.5)$$

These states form the free continuum, parametrized by the continuous parameter μ^2 . The spectral density $\rho(\mu^2)$ can then be interpreted as the density of states with respect to this

parameter. One can also introduce creation operators $a_{\mathbf{p},\mu}^\dagger$ for the free continuum such that

$$|\mathbf{p}, \mu^2\rangle = \sqrt{\frac{2E_\mu}{\rho(\mu)}} a_{\mathbf{p},\mu}^\dagger |0\rangle, \quad [a_{\mathbf{p},\mu}, a_{\mathbf{p}',\mu'}^\dagger] = (2\pi)^4 \delta^3(\mathbf{p} - \mathbf{p}') \delta(\mu^2 - \mu'^2) \quad (3.6)$$

which can also be used for the usual decomposition for the field Φ of the QFT³

$$\Phi(x) = \int \frac{d\mu^2}{2\pi} \sqrt{\rho(\mu)} \int \frac{d^3p}{(2\pi)^3 \sqrt{2E_\mu}} \left(a_{\mathbf{p},\mu}^\dagger e^{ip \cdot x} + a_{\mathbf{p},\mu} e^{-ip \cdot x} \right)_{p^0=E_\mu} \quad (3.9)$$

resulting in eq. (3.2). One can then use eq. (3.6) and eq. (3.9) to show that this field operator satisfies the equal-time commutation relation

$$[\dot{\Phi}(\mathbf{x}, t), \Phi(\mathbf{y}, t)] = -i\delta^3(\mathbf{x} - \mathbf{y}) \int \frac{d\mu^2}{2\pi} \rho(\mu). \quad (3.10)$$

Requiring that Φ is a canonically normalized field operator satisfying

$$[\dot{\Phi}(\mathbf{x}, t), \Phi(\mathbf{y}, t)] = -i\delta^3(\mathbf{x} - \mathbf{y}) \quad (3.11)$$

yields a normalization condition for the spectral density

$$\int_{\mu_0^2}^{\Lambda^2} \frac{d\mu^2}{2\pi} \rho(\mu) = 1, \quad (3.12)$$

where Λ is the UV cutoff of the effective theory in eq. (3.1). In practice, the spectral density ρ is decreasing rapidly at large μ , and the precise choice of Λ will not significantly affect our calculations.

The free continuum satisfies a completeness relation:

$$\int \frac{d\mu^2}{2\pi} \rho(\mu^2) \int \frac{d^3p}{(2\pi)^3} \frac{1}{2E_\mu} |\mathbf{p}, \mu^2\rangle \langle \mathbf{p}, \mu^2| = 1. \quad (3.13)$$

This is basically the standard one-particle completeness relation integrated over μ^2 weighted by $\rho(\mu^2)$, solidifying the picture of the entire continuum effectively acting as a single ordinary particle. The completeness relation can also be rewritten in a nice Lorentz-invariant form

$$\int \frac{d^4p}{(2\pi)^4} \rho(p^2) |\mathbf{p}, \mu^2\rangle \langle \mathbf{p}, \mu^2| = 1, \quad (3.14)$$

³For complex scalar Φ , we instead have

$$\Phi(x) = \int \frac{d\mu^2}{2\pi} \sqrt{\rho(\mu)} \int \frac{d^3p}{(2\pi)^3 \sqrt{2E_\mu}} \left(a_{\mathbf{p},\mu}^\dagger e^{ip \cdot x} + b_{\mathbf{p},\mu} e^{-ip \cdot x} \right)_{p^0=E_\mu} \quad (3.7)$$

with

$$[a_{\mathbf{p},\mu}, a_{\mathbf{p}',\mu'}^\dagger] = (2\pi)^4 \delta^3(\mathbf{p} - \mathbf{p}') \delta(\mu^2 - \mu'^2) = [b_{\mathbf{p},\mu}, b_{\mathbf{p}',\mu'}^\dagger] \quad (3.8)$$

being the only non-trivial commutation relations.

where $p_0 = E_\mu = \sqrt{\mathbf{p}^2 + \mu^2}$, and $p^2 = p_0^2 - \mathbf{p}^2$. The normalization of single-mode states consistent with completeness relation is given by

$$\langle \mathbf{p}', \mu'^2 | \mathbf{p}, \mu^2 \rangle = \frac{2E_\mu}{\rho(\mu^2)} (2\pi)^4 \delta^3(\mathbf{p} - \mathbf{p}') \delta(\mu^2 - \mu'^2). \quad (3.15)$$

In appendix A, we show that a gapped continuum can be obtained from a flat 5D space. In that simple example, completeness relation and associated state normalization are inherited from the standard 5D field theory, which indeed agree with eq. (3.13)-eq. (3.15).

Multi-mode states are built as direct products of these single-mode states, as usual. An interaction may be introduced to couple these states to the SM, and matrix elements are computed by the usual rules of perturbative QFT. For example, for a theory with eq. (3.1) and eq. (3.4), a scattering process $\text{SM} + \text{SM} \rightarrow \Phi(\mu_1) + \Phi(\mu_2)$ is described by a matrix element

$$\langle (\mathbf{p}_1, \mu_1^2), (\mathbf{p}_2, \mu_2^2) | T \exp \left(-i \int dt H_I(t) \right) | \mathbf{k}_A, \mathbf{k}_B \rangle_{\text{SM}} \equiv (2\pi)^4 \delta^4(k_1 + k_2 - p_1 - p_2) i\mathcal{M}. \quad (3.16)$$

A measurable cross section for this process will involve the production of the continuum over a finite region of the parameter μ , defined as

$$\sigma = \frac{1}{2E_A} \frac{1}{2E_B} \frac{1}{|v_A - v_B|} \int \frac{d\mu_1^2}{2\pi} \rho(\mu_1^2) \int \frac{d\mu_2^2}{2\pi} \rho(\mu_2^2) \int d\Pi_{\mu_1} d\Pi_{\mu_2} (2\pi)^4 \delta^4(k_1 + k_2 - p_1 - p_2) |\mathcal{M}|^2, \quad (3.17)$$

where the Lorentz-invariant phase space (LIPS) volume element is given as usual by

$$d\Pi_\mu = \frac{d^3p}{(2\pi)^3} \frac{1}{2E_\mu}. \quad (3.18)$$

In appendix C, we present a derivation of eq. (3.17) using a warped 5D model for a continuum and AdS/CFT correspondence.

The discussion above shows that in many respects the free continuum states are just like ordinary particles with mass μ^2 . The main difference is that the contribution of any single continuum state $|\mathbf{p}, \mu^2\rangle$ to any physical process will be negligible, and only the collective effect of the continuum will give finite contributions. Hence as stated above it is best to think of the continuum as a single smeared out particle. If all continuum states are accessible in a given scattering process, their contribution is similar to that of a single ordinary particle. However, if only a fraction of continuum states are kinematically accessible, the continuum will act as a “partial” particle, leading to suppressed scattering: DM direct detection offers a phenomenologically relevant example of this phenomenon.

3.2 Equilibrium Thermodynamics

Next we consider a dilute, weakly-coupled, spatially uniform gas made out of the free continuum states described above. We define the dimensionless phase-space density $f(\mathbf{p}, \mu^2)$ such that the number of excitations with mass-squared between μ^2 and $\mu^2 + d\mu^2$ is given

by

$$dN = V g \frac{d\mu^2}{2\pi} \rho(\mu^2) \int \frac{d^3 p}{(2\pi)^3} f(\mathbf{p}, \mu^2), \quad (3.19)$$

where g is the number of internal degrees of freedom and V is the volume occupied by the gas. (We will set $g = 1$ in the rest of this section to simplify the expressions.) The energy of the gas is given by

$$E = V \int \frac{d\mu^2}{2\pi} \rho(\mu^2) \int \frac{d^3 p}{(2\pi)^3} f(\mathbf{p}, \mu^2) E_\mu. \quad (3.20)$$

If interactions among continuum modes in the gas (either directly with each other, or through their interactions with some other, e.g. SM, gas) are strong enough to maintain them in thermal and chemical equilibrium with each other, the state of the gas can be completely characterized by two parameters, temperature $T = 1/\beta$ and chemical potential which we denote by η (to avoid confusion with the μ parametrizing the continuum). In this case, the phase-space density takes the standard Fermi-Dirac or Bose-Einstein form:⁴

$$f(\mathbf{p}, \mu^2) = \frac{1}{e^{\beta(E_\mu - \eta)} \pm 1} \approx e^{-\beta(E_\mu - \eta)} \quad (3.23)$$

where the two signs correspond to fermionic (+) and bosonic (−) free continuum states, and the second (Boltzmann) form applies in the limit of small occupation numbers. We will assume this limit below, and consider the case of zero chemical potential $\eta = 0$ as an example.

The free energy is given by

$$F = \frac{1}{\beta} V \int \frac{d\mu^2}{2\pi} \rho(\mu^2) \int \frac{d^3 p}{(2\pi)^3} \ln \left(1 \pm e^{-\beta E_\mu} \right). \quad (3.24)$$

Energy density u and pressure P can be found through the standard thermodynamic relations,

$$\begin{aligned} u &= \frac{1}{V} \left(\beta \frac{\partial F}{\partial \beta} \Big|_V + F \right), \\ P &= - \frac{\partial F}{\partial V} \Big|_\beta, \end{aligned} \quad (3.25)$$

⁴This can be proven by the standard method: we extremize the entropy with the constraints of energy and number density eq. (3.19) and eq. (3.20). These constraints can be enforced by means of Lagrange multiplier, and we need to extremize

$$\tilde{S} = S + \beta \left(\int \frac{d\mu^2}{2\pi} \rho \int \frac{d^3 p}{(2\pi)^3} f E - u \right) + \gamma \left(\int \frac{d\mu^2}{2\pi} \rho \int \frac{d^3 p}{(2\pi)^3} f - n \right). \quad (3.21)$$

The solution to $\frac{\delta \tilde{S}}{\delta f} = 0$ is

$$f^{\text{eq}} = e^{-(\gamma+1)} e^{-\beta E} \quad (3.22)$$

where the prefactor $e^{-(\gamma+1)}$ is fixed by the normalization.

and their explicit expressions are given by

$$\begin{aligned} u &= \int \frac{d\mu^2}{2\pi} \rho(\mu^2) \mathcal{U}(\mu^2), & \mathcal{U}(\mu^2) &= \int \frac{d^3p}{(2\pi)^3} \frac{E_\mu}{e^{\beta E_\mu} \pm 1}, \\ P &= \int \frac{d\mu^2}{2\pi} \rho(\mu^2) \mathcal{P}(\mu^2), & \mathcal{P}(\mu^2) &= \int \frac{d^3p}{(2\pi)^3} \frac{1}{e^{\beta E_\mu} \pm 1} \frac{p^2}{3E_\mu} \end{aligned} \quad (3.26)$$

where \mathcal{U} and \mathcal{P} are the equilibrium energy density and pressure of a gas of “normal” particles with mass-squared μ^2 . Roughly speaking, at temperatures above the gap scale, $T > \mu_0$, energy and pressure are dominated by modes with $\mu_0 < \mu < T$, which behave as a relativistic gas. At temperatures below the gap scale, $T < \mu_0$, energy and pressure are dominated by modes with $\mu \approx \mu_0$ (with details depending on the behavior of the spectral density in that region), which behave as a gas of non-relativistic particles. In this regime, the continuum gas can play the role of cold dark matter (CDM).

In principle, the spectral density itself can also be temperature dependent: $\rho(\mu^2, T)$. However, we expect that the thermal corrections will be of the order $\mathcal{O}(T/\Lambda)$, where $\Lambda \gg \mu_0$ is the cutoff scale of our description above which gapped continuum phase is replaced by a UV phase such as CFT. For this reason, in the following we will ignore this dependence, and revisit the validity of this assumption in section 6 when we discuss the concrete warped 5D model of gapped continuum.

3.3 Non-equilibrium Thermodynamics

We continue to consider a dilute, weakly-coupled gas of continuum states, but now do not assume that it is in thermal and/or chemical equilibrium. In this case the phase-space density is still sufficient to describe the gas, but it can now be a function of time: $f(\mathbf{p}, \mu^2, t)$. The time evolution of this quantity is described by the Boltzmann equation. For example, consider a model in which the continuum states can interact with SM states A, B through $2 \leftrightarrow 2$ scattering. In this case, the Boltzmann equation (in flat-space background) reads

$$\begin{aligned} E_\mu \frac{\partial f(\mathbf{p}, \mu^2, t)}{\partial t} &= -\frac{1}{2} \int \frac{d\mu'^2}{2\pi} \rho(\mu'^2) \int d\Pi_{\mu'} d\Pi_A d\Pi_B (2\pi)^4 \delta^4(k_A + k_B - p - p') \\ &\quad \times |\mathcal{M}|^2 (ff'(1 \pm f_A)(1 \pm f_B) - f_A f_B (1 \pm f)(1 \pm f')), \end{aligned} \quad (3.27)$$

where the usual sums over spin are included in $|\mathcal{M}|^2$. In the collision term on the right-hand side, k_A and k_B are the 4-momenta of the SM particles, p and p' are the 4-momenta of the continuum states (note that $p^2 = \mu^2$ and $p'^2 = \mu'^2$), $d\Pi$ are the LIPS volume elements defined in eq. (3.18), and \mathcal{M} is the scattering amplitude defined in eq. (3.16). In the limit of low occupation numbers which we will consider from now on, terms with \pm in front can be ignored. Generalization to gas in FRW background is straightforward. The only change is on the left-hand side, where the derivative $\partial/\partial t$ needs to be replaced with the covariant

version, giving

$$E_\mu \frac{\partial f(E, \mu^2, t)}{\partial t} - H |\mathbf{p}|^2 \frac{\partial f(E, \mu^2, t)}{\partial E} = -\frac{1}{2} \int \frac{d\mu'^2}{2\pi} \rho(\mu'^2) \int d\Pi_{\mu'} d\Pi_A d\Pi_B \\ \times (2\pi)^4 \delta^4(k_A + k_B - p - p') |\mathcal{M}|^2 (ff' - f_A f_B). \quad (3.28)$$

Here $H = \dot{a}/a$ is the Hubble parameter, $|\mathbf{p}|^2 = E^2 - \mu^2$, and we replaced p with E as the argument of f since 3D rotational invariance guarantees that f only depends on the magnitude of \mathbf{p} . Note that if the continuum originates from a 5D model, then using this form of the Boltzmann equation implies the assumption that the geometry of the bulk is fixed and only the 4D scale factor is still evolving.

4 Freeze-Out of Continuum Dark Matter

As an application of the above formalism, we study the process of freeze-out of continuum DM which can interact via $2 \leftrightarrow 2$ scattering with an SM particle with mass $m_{\text{SM}} \ll \mu_0$ (we set $m_{\text{SM}} = 0$ below). Before we give a more technical discussion, however, it seems instructive to note the following. Similarly to the particle DM, annihilation of continuum DM freezes out at $T \sim \frac{\mu_0}{10}$. At such low temperature, the continuum mass distribution is localized close to the gap scale, and it behaves more or less like a particle with mass $\sim \mu_0$. Therefore, as far as thermal freeze-out is concerned, the continuum DM is expected to be similar to particle DM. Below we confirm this by explicit computations and estimate the size of “continuum effects”.

4.1 Boltzmann Equation for Continuum Freeze-Out

For thermal freeze-out, there are two relevant reactions, *annihilation*

$$\text{DM}(\mu) + \text{DM}(\mu') \leftrightarrow \text{SM} + \text{SM} \quad (4.1)$$

and *quasi-elastic scattering* (QES)

$$\text{DM}(\mu) + \text{SM} \leftrightarrow \text{DM}(\mu') + \text{SM}. \quad (4.2)$$

If annihilation is in equilibrium, the continuum DM modes are at the same temperature T as the SM and at zero chemical potential. This will be the case, for sufficiently strong coupling between the SM and DM, at temperatures above the gap scale.⁵ Once $T \lesssim \mu_0$, however, the annihilation rate drops exponentially, and annihilations decouple (“freeze-out”). Note that the rate of quasi-elastic scattering of a DM state does not experience an exponential

⁵For any $T > \mu_0$, some of the DM states will be non-relativistic, since one can always go sufficiently far out on the tail of the continuum DM spectral density to ensure $\mu > T$. The equilibrium density of these states is exponentially suppressed, however they still remain in equilibrium and do not freeze out, since they can find annihilation partners among lighter DM states with $\mu < T$, whose equilibrium density is unsuppressed. Decay and inverse decay, $\text{DM}(\mu) \leftrightarrow \text{DM}(\mu') + \text{SM}$, also maintain equilibrium among the modes with different μ .

drop at these temperatures, and therefore the QES process continues to maintain thermal equilibrium between the SM and DM. It also maintains DM states of different masses in chemical equilibrium with each other, since the DM mass changes during QES. Therefore, during the freeze-out process, the DM modes are at the same temperature as the SM, T , and have a common (μ -independent) chemical potential η , which however is time-dependent and no longer vanishes. This means that in the freeze-out calculations we can assume

$$f_{\text{DM}} = e^{-\beta(E_\mu - \eta(t))}, \quad f_{\text{SM}} = e^{-\beta|p|}. \quad (4.3)$$

The effective DM number density is given by

$$n = \int \frac{d\mu^2}{2\pi} \rho(\mu^2) \int \frac{d^3p}{(2\pi)^3} f_{\text{DM}}. \quad (4.4)$$

If n_{eq} denotes the value of n with $\eta = 0$ (i.e. in chemical equilibrium with the SM), then $n = n_{\text{eq}} e^{\beta\eta}$, leading to a useful expression of the DM phase space density in terms of the number densities

$$f_{\text{DM}} = \frac{n}{n_{\text{eq}}} e^{-\beta E_\mu}. \quad (4.5)$$

Integrating both sides of the Boltzmann equation eq. (3.28) with respect to $\int \frac{d\mu^2}{2\pi} \rho(\mu^2) \int \frac{d^3p}{(2\pi)^3}$, and using eq. (4.5) on the right-hand side and the usual integration-by-parts trick in the second term on the left-hand side, yields the equation for time evolution of DM number density becomes,

$$\frac{\partial n}{\partial t} + 3Hn = -\langle \sigma v \rangle (n^2 - n_{\text{eq}}^2), \quad (4.6)$$

where we defined

$$\begin{aligned} \langle \sigma v \rangle &= \frac{1}{n_{\text{eq}}^2} \int \frac{d\mu^2}{2\pi} \rho(\mu^2) \int \frac{d\mu'^2}{2\pi} \rho(\mu'^2) \int d\Pi_\mu d\Pi_{\mu'} d\Pi_A d\Pi_B \\ &\times (2\pi)^4 \delta^4(k_A + k_B - p - p') |\mathcal{M}|^2 \exp(-\beta(E_A + E_B)). \end{aligned} \quad (4.7)$$

It is interesting to note that eq. (4.6) is identical to that of the usual particle cold relic, and hence the relic density is given by the usual expression found in e.g. Kolb and Turner [50]. All effects of the continuum physics are encoded in the calculation of $\langle \sigma v \rangle$.

4.2 Freeze-Out in a Toy Model

As an illustration, consider a toy model described by eq. (3.1) and eq. (3.4) where the DM and “SM” are both scalars, coupled through a 4-point coupling independent of the DM-mode masses. For simplicity, we set $m_h = 0$ in this illustrative example. The tree-level

matrix element in eq. (4.7) is then simply $\mathcal{M} = \lambda$. An explicit calculation yields⁶

$$\langle \sigma v \rangle = \frac{\lambda^2}{32\pi} \left(\frac{I_1(\beta)}{I_2(\beta)} \right)^2. \quad (4.10)$$

Here we defined

$$I_n(\beta) \equiv \int \frac{d\mu^2}{2\pi} \rho(\mu^2) \mu^n K_n(\beta\mu), \quad (4.11)$$

where K_n is the modified Bessel function of the second kind. In eq. (4.10) the I_1^2 in the numerator is the result of performing the phase space integrals for the continuum DM, while the I_2^2 in the denominator originates from the integrals corresponding to the $1/n_{\text{eq}}^2$ factor in eq. (4.7). As explained above, freeze-out occurs when the temperature drops below the gap scale, so we can approximate the Bessel functions at large argument. This yields

$$I_n(\beta) \approx \sqrt{\frac{\pi}{2\beta}} \int_{\mu_0}^{\infty} \frac{d\mu}{\pi} \rho(\mu^2) \mu^{n+1/2} e^{-\beta\mu}. \quad (4.12)$$

To make it even more explicit, let's assume a specific form for spectral density. Motivated by 5D model building (see section 6), we use

$$\rho(\mu^2) = \frac{\rho_0}{\mu_0^2} \left(\frac{\mu^2}{\mu_0^2} - 1 \right)^{1/2}, \quad (4.13)$$

where ρ_0 is a dimensionless constant. In section 6 we show that this is indeed the form of the spectral density near the gap scale, and in appendix B we present a more general argument for this. With this assumption, the integrals in (4.12) can be evaluated using the saddle-point approximation, giving⁷

$$\langle \sigma v \rangle = \frac{\lambda^2}{32\pi\mu_0^2} + \mathcal{O}\left(\frac{T}{\mu_0}\right). \quad (4.14)$$

Here, the term $\mathcal{O}(T/\mu_0)$ encodes the corrections due to the continuum nature of our DM and is typically expected to be of the order of $\sim 10\%$. Note that the result is independent of ρ_0 , and depends only weakly upon the assumed functional form of spectral density (although may need to be modified if it changes very rapidly or is very suppressed near the gap).

⁶We used an integral representation

$$K_n(z) = \frac{\pi^{1/2} \left(\frac{z}{2}\right)^n}{\Gamma\left(n + \frac{1}{2}\right)} \int_1^{\infty} dt e^{-zt} (t^2 - 1)^{n-1/2}, \quad (4.8)$$

Using this, it is straightforward to show that

$$\int d\Pi_{\mu} e^{-\beta E_{\mu}} = \frac{1}{4\pi^2} \mu \beta^{-1} K_1(\mu\beta), \quad \int \frac{d^3 p}{(2\pi)^3} e^{-\beta E_{\mu}} = \frac{1}{2\pi^2} \mu^2 \beta^{-1} K_2(\mu\beta). \quad (4.9)$$

The second identity is easily obtained by taking a partial derivative with respect to β of the first identity and using $\frac{\partial(z^{-n} K_n(z))}{\partial z} = -z^{-n} K_{n+1}(z)$.

⁷This result is valid as long as the saddle point is near the gap scale, $\mu_{\text{saddle}} \approx \mu_0 + \mathcal{O}(T)$, and independent of n of $I_n(\beta)$.

We can also explicitly verify that assumptions made in the derivation of Eq. (4.6) indeed hold in this toy model. Let Γ_{an} and Γ_{QES} denote the rates at which a DM state of energy E undergoes annihilation and QES respectively. Estimating the rates in this model gives $\Gamma_{\text{an}} \sim \Gamma_{\text{QES}} \gg H$ for $T > \mu_0$ (assuming $\lambda \sim \mathcal{O}(1)$), so both reactions are active and maintain thermal and chemical equilibrium between SM and DM. However when $T < \mu_0$, the ratio $\Gamma_{\text{an}}/\Gamma_{\text{QES}}$, which is roughly the ratio of number density of non-relativistic state to that of relativistic state $n_{\text{NR}}/n_{\text{R}}$, becomes

$$\frac{\Gamma_{\text{an}}}{\Gamma_{\text{QES}}} \sim \left(\frac{\mu_0}{T}\right)^{3/2} e^{-\mu_0/T}, \quad (4.15)$$

so that annihilations decouple well before QES, as assumed. At $T < \mu_0$, QES reaction with incoming DM mode of mass μ can have final-state DM state in the mass range $[\mu_0, \mu + T]$, so that chemical equilibrium among the DM modes of all possible masses is maintained. This justifies our assumption that the DM chemical potential η is μ -independent during the freeze-out.

5 WIC model using the Vector Boson Portal

We are now ready to present a fully realistic WIC model based on the Z/W portal. In this section we will be discussing it based on a 4D description assuming that a gapped continuum mode is readily available and can be coupled to the SM. The resulting theory is presented in section 5.1, while the evaluation of the dark matter relic density in this theory is in section 5.2 below. A UV completion of this theory can be obtained using a warped extra dimensional construction with a non-trivial scalar field profile, which will be discussed in section 6.

5.1 4D Effective Z-portal Model

We denote the field corresponding to the continuum DM by Φ , which is assumed to be a complex scalar with no SM gauge quantum numbers. First we take it as a 4D field with an unusual “kinetic term” corresponding to the gapped continuum, while in the next section we will lift it to the boundary value of a 5D field. In order to obtain non-vanishing interactions of the continuum DM with the SM W, Z bosons we will mix it with another complex scalar field χ (with a canonical kinetic term) which is a doublet under $SU(2)_L$ and carries $U(1)_Y$ charge $-1/2$.⁸ This mixing is possible in the presence of the Higgs VEV. We assume that the χ field itself does not break the electroweak symmetry, hence its mass is a free parameter

⁸One may wonder why we don’t just couple Φ directly to Z and W by giving it SM gauge charges. In fact, this is possible. The mixing with mediator χ in this 4D construction is just to avoid continuum partners of Z and W , which are required in the direct coupling case according to 5D consistency, and yield a more complicated theory.

and can be taken to be relatively high $m_\chi \gg v$. The Lagrangian of the theory is

$$\mathcal{L} = \mathcal{L}_{\text{SM}} + \mathcal{L}_\Phi + \mathcal{L}_\chi + \mathcal{L}_{\text{int}} \quad (5.1)$$

$$\mathcal{L}_\Phi = \Phi^\dagger(p) \Sigma(p^2) \Phi(p) \quad (5.2)$$

$$\mathcal{L}_\chi = (D_\mu \chi)^\dagger (D^\mu \chi) - m_\chi^2 \chi^\dagger \chi \quad (5.3)$$

$$\mathcal{L}_{\text{int}} = -\lambda \Phi \chi H + \text{c.c.} \quad (5.4)$$

The quadratic action of Φ describes the continuum spectrum through the spectral density $\rho(p^2)$ defined by

$$\rho(p^2) = -2\text{Im}\Sigma^{-1}(p^2). \quad (5.5)$$

The covariant derivative appearing in \mathcal{L}_χ includes couplings to the SM W and $U(1)_Y$ gauge bosons. We will assume that the temperature of the Universe is low enough that a Higgs VEV has already formed, $T < v$, and also $T < m_\chi$. When the Higgs gets a vev, \mathcal{L}_{int} -term induces “mass mixing” between continuum states created by Φ and the neutral components of χ .⁹ In the standard case where Φ describes a single massive particle (as opposed to gapped continuum), the mass eigenstates would be given by the usual expressions

$$\tilde{\Phi} = \cos \alpha \Phi + \sin \alpha \chi^0, \quad \tilde{\chi}^0 = -\sin \alpha \Phi + \cos \alpha \chi^0.$$

The mixing angle would be

$$\tan 2\alpha = \frac{\sqrt{2}\lambda v}{m_\chi^2 - m_\Phi^2},$$

where $v = 246$ GeV. In the continuum case, we can get a similar result by simply integrating out χ^0 using its EoM (assuming χ is sufficiently heavy, in particular $m_\chi \gg \mu_0$ and the temperature is low enough that only states close to μ_0 will be relevant). In this case the EoM for χ^0 implies

$$\chi^0 = -\frac{\lambda v}{\sqrt{2}\square + m_\chi^2} \Phi \quad (5.6)$$

where $\square \equiv \partial_\mu \partial^\mu$. Substituting this back into the action results in an effective action for Φ with mixing angles dependent on the mode mass μ :

$$\tan 2\alpha_\mu = \frac{\sqrt{2}\lambda v}{m_\chi^2 - \mu^2}. \quad (5.7)$$

Since we are assuming that $\mu \ll m_\chi$ for all relevant μ we may safely drop the μ -dependence in the mixing angle. The couplings of continuum modes with $p^2 = \mu^2$ to the SM Z and W gauge bosons are inherited from its mixing with χ^0 . The effective Lagrangian describing

⁹Charged components of χ have mass $m_\chi \gg \mu_0$ and will not play a role in DM phenomenology.

these couplings are given by (dropping the μ -dependence in the mixing angle)

$$\mathcal{L}_{\Phi-Z,W} = \sin^2 \alpha \left[-\frac{i}{2} g_Z \left(\partial_\mu \Phi^\dagger \Phi - \Phi^\dagger \partial_\mu \Phi \right) Z^\mu + \frac{1}{4} g_Z^2 \Phi^\dagger \Phi Z_\mu Z^\mu + \frac{1}{2} g^2 \Phi^\dagger \Phi W_\mu^+ W^{-\mu} \right] \quad (5.8)$$

where g, g' are the standard $SU(2)_L \times U(1)_Y$ couplings, and $g_Z = \sqrt{g^2 + g'^2}$. At first glance, this equation simply describes a complex scalar coupled to Z and W with extra factor of mixing angle $\sin^2 \alpha$. We emphasize, however, that Φ excites a whole set of free continuum states with the probability governed by the spectral density $\rho(\mu^2)$. Hence, eq. (5.8) contains couplings of the continuum modes for all values of $p^2 = \mu^2$ to W and Z .

5.2 Relic abundance of continuum Z -portal DM

In this section, we compute rates for processes relevant for the thermal freeze-out of continuum DM introduced above. We then show a region of parameter space $(\sin \alpha, \mu_0)$ that reproduces observed relic density. The spectral density is assumed to have the generic form in eq. (4.13), although as remarked in section 4 the relic density is essentially independent of this assumption.

Thermal-relic WIC occurs when the DM sector is in thermal and chemical equilibrium with SM at high temperature, at least $T \sim \text{TeV}$. This requirement places a lower bound on the effective coupling, and hence on $\sin \alpha$:

$$\Gamma = \langle \sigma v \rangle n \sim \frac{g_Z^4 \sin^4 \alpha}{8\pi} T \gtrsim \frac{T^2}{M_{\text{Pl}}} \quad \rightarrow \quad \sin \alpha \gtrsim 10^{-4} \left(\frac{\text{TeV}}{M_{\text{Pl}}} \right)^{1/4}. \quad (5.9)$$

Below we assume that this bound is satisfied and thermal freeze-out occurs. The observed relic density indicates values of $\sin \alpha$ that are easily consistent with this bound, so the calculation is self-consistent.

We now move on to the discussion of thermal freeze-out. Recall that the quasi-elastic scattering process which establishes thermal equilibrium between DM sector and SM decouples much later than the annihilations (see section 4). Therefore, when thermal freeze-out occurs we can safely assume that DM sector is in thermal equilibrium with SM.

As discussed around eq. (4.6) and eq. (4.7) the Boltzmann equation for continuum is the same as particle DM except that, crucially, the thermal averaged rate includes averaging over the continuum spectrum. The relevant annihilation processes depend on the size of gap scale μ_0 :

- (1) $\mu_0 < m_W$: The dominant process is $\phi\phi^* \rightarrow f\bar{f}$ via the s-channel Z exchange. Here, f denotes SM fermions (excluding top quark). The rate is given by

$$\langle \sigma v \left(\phi\phi^* \rightarrow Z^{(*)} \rightarrow f\bar{f} \right) \rangle \approx \frac{g_Z^2 \sin^4 \alpha v_{\text{rel}}^2}{128\mu_0^2} \frac{\Gamma_Z}{m_Z} \left[\left(1 - \frac{m_Z^2}{4\mu_0^2} \right)^2 + \frac{m_Z^2 \Gamma_Z^2}{16\mu_0^4} \right]^{-1}. \quad (5.10)$$

The appearance of the relative velocity v_{rel}^2 shows that this process is p-wave. The factor Γ_Z/m_Z comes from the $Z \rightarrow f\bar{f}$ vertex of the Feynman diagram, and the last

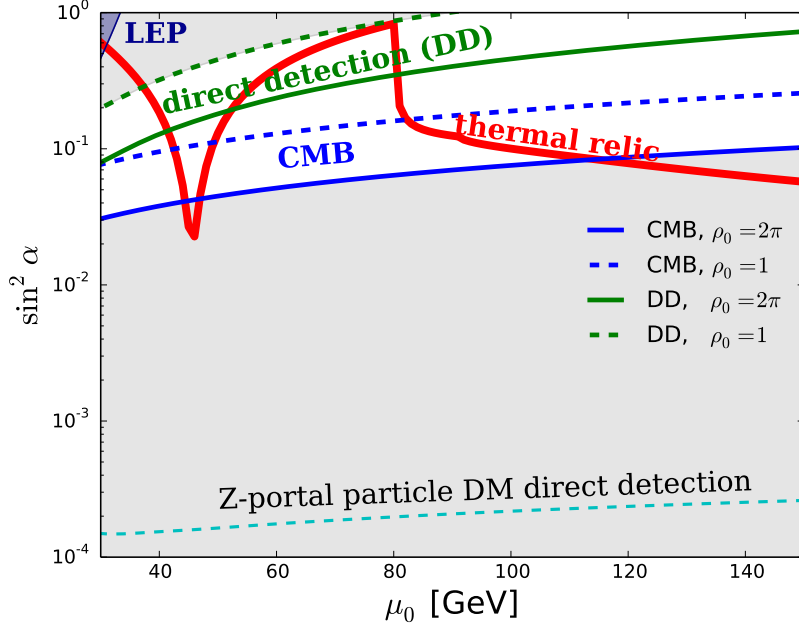


Figure 3. The parameter space of the Z-portal WIC DM. The red curve corresponds to the observed relic density for this model. The region below the solid (dashed) blue lines is ruled out by the CMB observations for $\rho_0 = 2\pi$ ($\rho_0 = 1$). The region above the solid (dashed) green line is constrained by the XENON1T direct detection experiment [23] for $\rho_0 = 2\pi$ ($\rho_0 = 1$). For comparison, the Z-portal particle DM direct detection constraint is shown in the cyan dashed line. LEP bound from on-shell decays $Z \rightarrow \phi\phi^*$ [51] is also shown ($\rho_0 = 2\pi$). The details of these bounds are discussed in the companion paper [43].

factor in the square bracket is the Z propagator. When $\mu_0 \ll \frac{m_Z}{2}$, one sees that $\langle\sigma v\rangle \propto \frac{\sin^4 \alpha \mu_0^2}{m_Z^4}$, and so for the correct relic density $\sin \alpha$ decreases as μ_0 increases. On the other hand, for $\frac{m_Z}{2} \ll \mu_0 < m_Z$, instead we get $\langle\sigma v\rangle \propto \frac{\sin^4 \alpha}{\mu_0^2}$. Hence, $\sin \alpha$ increases with μ_0 . These features are seen in fig. 3.

- (2) $\mu_0 \sim m_W$: In this regime, in addition to $\phi\phi^* \rightarrow f\bar{f}$, the three-body process, $\phi\phi^* \rightarrow WW^* \rightarrow W\ell\bar{\nu}$ can make a significant contribution. This, however, will be only relevant for μ_0 very close to m_W and we leave its explicit computation for a future investigation. For this reason, we warn that an $\mathcal{O}(1)$ (at most) correction may be required to the relic density curve in fig. 3 for $\mu_0 \approx m_W$.
- (3) $m_W < \mu_0 < m_Z$: Now, a W pair can be produced on-shell: $\phi\phi^* \rightarrow W^+W^-$. The rate is estimated to be

$$\langle \sigma v (\phi \phi^* \rightarrow W^+ W^-) \rangle_{\text{ct}} \approx \frac{g^4 \sin^4 \alpha}{128 \pi \mu_0^2} \sqrt{1 - \frac{1}{y}} (4y^2 - 4y + 3), \quad (5.11)$$

$$\langle \sigma v (\phi \phi^* \rightarrow W^+ W^-) \rangle_{\text{s}} \approx \frac{g^4 \sin^4 \alpha v_{\text{rel}}^2}{96 \pi \mu_0^2} \sqrt{1 - \frac{1}{y}} \frac{4y^2 + 20y + 3}{y^2} \left(4 - \frac{1}{x}\right)^{-2} \quad (5.12)$$

where $y = \mu_0^2/m_W^2$ and $x = \mu_0^2/m_Z^2$. The first contribution comes from a contact interaction, while the second is from a s-channel Z exchange.¹⁰ Eq. (5.11) is an s-wave process while Eq. (5.12) is p-wave. As $\mu_0 \gg m_W$, the rates become $\langle \sigma v \rangle_{\text{ct}} \propto \frac{\sin^4 \alpha}{m_W^4} \mu_0^2$ and $\langle \sigma v \rangle_{\text{s}} \propto \frac{\sin^4 \alpha}{\mu_0^2}$. This means that at $\mu_0 \gg m_W^2$, the contact contribution dominates and $\sin \alpha$ drops with increased μ_0 for fixed relic density. As μ_0 is brought close to m_W (so $y \approx 1$), both processes get phase-space suppression as captured by $\sqrt{1 - 1/y}$. The observed relic abundance then is achieved by taking larger and larger $\sin \alpha$. These features are all seen in fig. 3.

- (4) $\mu_0 > m_Z$: Finally, for μ_0 larger than the Z mass, a pair of Z bosons can be produced on-shell. This process is due to the contact interaction and the rate is

$$\langle \sigma v (\phi \phi^* \rightarrow ZZ) \rangle \approx \frac{g_z^4 \sin^4 \alpha}{256 \pi \mu_0^2} \sqrt{1 - \frac{1}{x}} \left[4x^2 - 4x + 3 - 8x(x-1) \sin^2 \alpha + \frac{16x^2(x-1)^2 \sin^4 \alpha}{(2x-1)^2} \right]. \quad (5.13)$$

Here, again, $x = \mu_0^2/m_Z^2$. This process is s-wave as $\langle \sigma v \rangle \propto v_{\text{rel}}^0$. We also note that at large x , the expression in the square bracket behaves as $[\dots] \rightarrow x^2 \cos^4 \alpha$. The growth with x indicates that longitudinal Z modes do not decouple. This is in fact required by the Goldstone boson equivalence theorem due to non-vanishing $\Phi \chi H$ coupling in this model. (If the DM were directly coupled under the gauge symmetry, we would have $\sin \alpha = 1$ and in fact $|\mathcal{M}|^2$ does not grow at large x in this limit, as expected.) For $x \gg 1$, the rate becomes $\langle \sigma v \rangle \propto \frac{\sin^4 2\alpha}{m_Z^4} \mu_0^2$, same scaling as in the case of WW final state above.

The region of parameter space where the observed relic density is reproduced is shown in fig. 3: roughly, for $\mu_0 \sim 100$ GeV, the effective coupling $g_{\text{eff}} \approx g \sin^2 \alpha \gtrsim 10^{-2}$ is required. This is similar to ordinary particle DM with a Z-portal. The crucial difference is that while for ordinary particle the coupling of this size is completely ruled out by direct detection experiments, in the case of WIC this bound is much weaker due to the suppression of direct detection rates discussed in section 2. The bounds from direct detection, as well as from the consistency of ionization history of the universe in the presence of late-time WIC decays, are discussed in the companion paper [43] and are summarized in fig. 3. Z-portal WIC dark matter is consistent with all experimental bounds.

¹⁰The absence of the interference between the contact and s-channel contributions to the matrix element is due to the fact that the former is purely real while the latter is purely imaginary.

6 Continuum Spectral Density and UV-Complete WIC Model from a Warped Spacetime

Finally we present a realistic implementation of the continuum DM scenario with a Z-portal in a local and unitary 5D theory. The main goal is to construct a UV completion of the 4D effective theory shown in section 5.1 and used for the relic density calculation in section 5.2. We start by recalling the soft-wall construction of a gapped continuum in 5D warped space following [32]. In section 6.2 we examine the detailed properties of the resulting spectral density, paying particular attention to the behavior of ρ close to the gap, which turns out to be crucial for the dark matter phenomenology. Finally in section 6.3 we present an explicit 5D model whose 4D effective theory (by integrating out the bulk) matches to the effective theory given in section 5.1, and which makes a concrete prediction for the form of the spectral density $\rho(\mu^2)$. The holographic dual description of our 5D gapped continuum in terms of strongly coupled CFT is discussed in appendix C.

6.1 The Cabrer-von Gersdorff-Quiros (CGQ) Background

In the warped 5D setup we will have a 3-brane placed at the position $z = R$, which from the point of view of the bulk field will be a UV brane cutting off the space. Toward the IR the extra dimension is non-compact, supplemented by a *background scalar field* $\varphi(y)$, whose back-reaction is responsible for a so-called soft-wall, resulting in a finite proper length for the extra dimension. Note that in this paper we are not trying to solve the Higgs hierarchy problem, but merely provide a complete construction of a gapped continuum. Hence our UV scale defined by the location of the UV brane is not exponentially larger than the weak scale, but rather comparable to it. (If we did try to embed this setup into a traditional Randall-Sundrum-type warped extra dimensional model [52] we would need to extend it beyond our UV brane. In fact in that UV complete theory the brane we are using as a UV cutoff here would actually be identified with the traditional IR brane of RS, and a new UV brane would have to be introduced in the far UV at scales exponentially higher than the weak scale.) Another point we want to mention is that below we will work in zero temperature background. In the context of cosmology, such a zero temperature geometry will arise after a thermal phase transition around $T \lesssim T_c$ (assuming not highly super-cooled phase transition). In dual CFT description, at $T > T_c$, the theory is in hot CFT phase (dual to AdS black hole phase in 5D), while at $T < T_c$ it is in gapped continuum phase. A non-trivial cosmology of gapped continuum is possible provided $\mu_0 < T_c$ which we assume. We note that at finite $T < T_c$, the geometry is not quite yet that of zero temperature, but rather thermal AdS where the temporal direction is compactified with radius $\sim 1/T$. It is then expected that spectral density computed in such a background will exhibit T -dependence. On the other hand, naive dimensional analysis suggests that thermal corrections are suppressed as $\mathcal{O}(T/T_c)$ (note that $T_c \approx \Lambda$ where Λ is cutoff scale). In this work, we ignore such thermal corrections.

The 5D action of the coupled scalar-gravity system is given by

$$S = \int d^5x \sqrt{g} \left(-M^3 R + \frac{1}{2} g^{MN} (\partial_M \varphi) (\partial_N \varphi) - V(\varphi) \right) - \int d^4x \sqrt{g^{\text{ind}}} V_4(\varphi) \quad (6.1)$$

where M^3 is the 5D Planck mass and we are using the metric signature $(+, -, -, -, -)$.¹¹

Using the proper distance as the coordinate along the extra dimension we parametrize the metric as

$$ds^2 = e^{-2A(y)} dx^2 - dy^2 \quad (6.2)$$

where $A(y)$ is the warp factor. While solving the coupled Einstein-scalar equations analytically in general is rather challenging, there is a special case when the coupled second order equations simplify to first order ordinary differential equations which can be analytically solved. Such a simplification occurs when the scalar potential can be given in terms of a superpotential W via the relation [55, 56]

$$V(\varphi) = \frac{1}{8} \left(\frac{\partial W}{\partial \varphi} \right)^2 - \frac{1}{12M^3} W^2. \quad (6.3)$$

In terms of the superpotential, the bulk EoMs take a simple form

$$\frac{d\varphi}{dy} = \frac{1}{2} \frac{\partial W}{\partial \varphi}, \quad \frac{dA}{dy} = \frac{1}{12M^3} W. \quad (6.4)$$

The superpotential leading to the desired 5D background¹² is given by [32],

$$W(\varphi) = 12kM^3 \left(1 + e^{\varphi/\sqrt{6M^3}} \right) \quad (6.5)$$

where k is the AdS curvature scale asymptotically away from the soft wall. The solution of the first order differential equations yield the background

$$A(y) = ky - \log \left(1 - \frac{y}{y_s} \right), \quad (6.6)$$

and

$$\varphi(y) = -\sqrt{6M^3} \log(k(y_s - y)). \quad (6.7)$$

It is observed that there is a singularity located at y_s and it corresponds to the finite distance location of the curvature singularity where the spacetime ends in the y coordinates (corresponding to $z \rightarrow \infty$ in the conformally flat coordinates). It is also seen that for $y \ll y_s$, $A \rightarrow ky$ and the geometry is just AdS_5 . The beauty of this solution is that it fully includes the backreaction of the metric to the presence of the scalar field - which is indeed the origin of the actual curvature singularity.

¹¹Since our spacetime manifold has a boundary, the Gibbons-Hawking-York (GHY) boundary term is required so that the variational principle for gravity is well-defined [53, 54]. Its explicit form is not needed for our discussion and we ignore it.

¹²Note that this is a special case of a class of superpotentials parametrized as $W = 12kM^3 \left(1 + e^{\nu\varphi/\sqrt{6M^3}} \right)$. For $\nu > 1$ one has a discrete spectrum, while for $\nu < 1$ a continuum without a gap. The critical value $\nu = 1$ corresponds to a gapped continuum of the sort we are considering.

6.2 Realistic Gapped Continuum Spectral Density

The gapped continuum is obtained by considering additional fields (scalar, vector or fermion) in this background¹³. To be concrete, we consider the simplest case of a scalar continuum with a mass gap, by introducing an additional scalar field Φ (which would play the role of dark matter) in this 5D set-up with the assumption of a stabilizing (e.g. Z_2) symmetry. The Lagrangian for this additional scalar is

$$\mathcal{L} = \sqrt{g} \left[g^{MN} D_M \Phi^\dagger D_N \Phi - m^2 |\Phi|^2 \right], \quad (6.8)$$

where for simplicity we choose to set brane localized potentials to zero and ignore scalar self-interaction terms in the bulk. By means of integration by parts along the fifth dimension, the bulk action can be written so that it is proportional to the bulk EoM. This is a useful representation since it leads to a vanishing bulk action once the bulk field is evaluated at its classical solution. The integration by parts, however, induces a UV-localized term

$$\Delta S_{\text{UV}} = \int_{\text{UV}} d^4x \Phi^\dagger \partial_y \Phi, \quad (6.9)$$

which then turns into the (holographic) effective action [57, 58] once the bulk is integrated out at tree level.

Using a field redefinition $\Psi(p, y) = e^{-2A(y)} \Phi(p, y)$ where $p = \sqrt{p^2}$, the bulk EoM in the mixed momentum-position coordinates becomes

$$\left(-\partial_y^2 + \hat{V}(y) \right) \Psi(p, y) = e^{2A(y)} p^2 \Psi(p, y) \quad (6.10)$$

where the potential $\hat{V}(y)$ is given in terms of the warp factor by

$$\hat{V}(y) = m^2 + 4 \left(A'(y) \right)^2 - 2A''(y). \quad (6.11)$$

Here $()'$ denotes the derivative with respect to y . Further insight into the modes in this potential can be gained by transforming eq. (6.10) into a Schrödinger form, which can be achieved by going into the conformally flat z coordinates via $dz/dy = e^A$ and an additional rescaling $\psi = e^{A/2} \Psi$. In this frame, the bulk EoM turns into the standard Schrödinger equation

$$-\ddot{\psi} + V(z)\psi = p^2 \psi \quad (6.12)$$

with the potential given by

$$V(z) = m^2 e^{-2A} + \frac{9}{4} \left(\dot{A} \right)^2 - \frac{3}{2} \ddot{A}. \quad (6.13)$$

Here $\dot{()}$ denotes the derivative with respect to the conformal coordinate z . An explicit

¹³For the case of the fermions, one needs to introduce an additional Yukawa-like coupling to the background scalar field φ to yield a gapped continuum. Without such coupling the continuum would start at zero.

expression for V can be obtained using eq. (6.6)

$$V(z) = \frac{e^{-2ky}}{4y_s^2} \left[4m^2(y_s - y)^2 + 15(1 + k(y_s - y))^2 - 6 \right]. \quad (6.14)$$

It is understood that y should be expressed in terms of the conformally flat coordinate $y(z)$ via the transformation $dz/dy = e^A$. The potential approaches a constant

$$\mu_0^2 = \frac{9}{4y_s^2} e^{-2ky_s} \quad (6.15)$$

for $y \rightarrow y_s$, providing the mass gap for the continuum. Once the solution to the EoM, eq. (6.12) and eq. (6.13), is found, we obtain the boundary (or holographic) effective action

$$\begin{aligned} S_{\text{eff}} &= \int_{\text{UV}} d^4x \Phi^\dagger(x, y) \partial_y \Phi(x, y)|_{y=0} \\ &= \int_{\text{UV}} d^4x \psi^\dagger(x, z) e^{\frac{5}{2}A(z)} \partial_z \left(e^{\frac{3}{2}A(z)} \psi(x, z) \right) \Big|_{z=R} \\ &= \int_{\text{UV}} \frac{d^4p}{(2\pi)^4} \frac{1}{R} \hat{\Phi}^\dagger(p) e^{\frac{5}{2}A(z)} \partial_z \left(e^{\frac{3}{2}A(z)} \frac{f(z, p)}{f(R, p)} \right) \Big|_{z=R} \hat{\Phi}(p) \end{aligned} \quad (6.16)$$

where in the last line we performed the mode decomposition

$$\psi(p, z) = R^{-1/2} \frac{f(z, p)}{f(R, p)} \hat{\Phi}(p). \quad (6.17)$$

Here, R is the location of the UV brane and we defined 4D field $\hat{\Phi}(p)$. This effective action is in fact identical to eq. (3.1), the starting point of our discussion of the free continuum in section 3, with

$$\Sigma(p) = \frac{C}{R} e^{\frac{5}{2}A(R)} \partial_z \left(e^{\frac{3}{2}A(z)} \frac{f(z, p)}{f(R, p)} \right) \Big|_{z=R}. \quad (6.18)$$

The (constant) wavefunction renormalization factor C is required to ensure that the 4D field $\hat{\Phi}$ satisfies the complex-field analogue of the equal-time commutation relation eq. (3.11), and is fixed by imposing the normalization condition in eq. (3.12). The associated spectral density is defined by eq. (3.3). We emphasize that this effective action was obtained starting from a local and unitary scalar field theory propagating in a self-consistent 5D background space.

We can now find the expression for the spectral density close to the mass gap μ_0 . While the above potential $V(z)$ cannot be obtained analytically, the asymptotic form of the potential for $z \rightarrow \infty$ needed for the spectral density near the mass gap can be found explicitly. As $y \rightarrow y_s$, we may get the expression for $k(y_s - y)$ in terms of z by noting that the integrand in

$$z = \int dy \frac{y_s}{y_s - y} e^{ky} \quad (6.19)$$

has a rapidly varying factor $1/(y_s - y)$ and we may treat e^{ky} to be approximately constant. Performing the integral with this approximation yields

$$z = -y_s e^{ky_s} \log(k(y_s - y)) = -\frac{3}{2\mu_0} \log(k(y_s - y)) \rightarrow k(y_s - y) = e^{-\frac{2}{3}\mu_0 z} \quad (6.20)$$

where we used eq. (6.15). Hence, the potential eq. (6.14) can be written near $z \rightarrow \infty$ as

$$V(z) \rightarrow \mu_0^2 \left[1 + \frac{10}{3} e^{-\frac{2}{3}\mu_0 z} + \left(\frac{4m^2}{9k^2} + \frac{15}{9} \right) e^{-2\frac{2}{3}\mu_0 z} \right]. \quad (6.21)$$

The solution of the Schrödinger equation for the asymptotic potential (assuming an outgoing wave boundary condition $\psi \rightarrow e^{ikz}$ for $z \rightarrow \infty$, and setting the bulk mass to zero for simplicity) can also be explicitly found in terms of a generalized Laguerre polynomial:

$$\psi(z, \mu) = D L_l^n(3\sqrt{5}e^{-2z\mu_0/3}) \exp\left(\frac{3}{2}\sqrt{1 - \frac{\mu^2}{\mu_0^2}} \log\left(e^{-\frac{2\mu_0 z}{3}}\right) - \frac{3\sqrt{5}}{2}e^{-\frac{2\mu_0 z}{3}}\right), \quad (6.22)$$

with $l = -(3\sqrt{5} + 1)/2 - 3/2\sqrt{1 - \mu^2/\mu_0^2}$, $n = 3\sqrt{1 - \mu^2/\mu_0^2}$, and an arbitrary coefficient D is fixed by the normalization condition. The spectral density is related to the brane-to-brane propagator (with the location of the brane assumed at $z = R$) given by $G(R, R; p) = \Sigma(p)^{-1}$ (with $\Sigma(p)$ given in eq. (6.18)) and is given as

$$\rho(p) = -2\text{Im } \Sigma(p)^{-1}. \quad (6.23)$$

Since the potential in eq. (6.21) is only valid for large $z \rightarrow \infty$ which is relevant for modes $\mu^2 \sim \mu_0^2$ we can expand the arguments of the Laguerre polynomial around the mass gap (with an expansion $\sqrt{\mu^2/\mu_0^2 - 1} \ll 1$) to obtain the approximate form of the spectral density near the mass gap $\mu \approx \mu_0$,

$$\rho(\mu^2) = \frac{\rho_0}{\mu_0^2} \left(\frac{\mu^2}{\mu_0^2} - 1 \right)^{1/2}, \quad (6.24)$$

where ρ_0 is a dimensionless constant. We can in fact show in a model independent way that around the mass gap this is indeed the expected form of the spectral density in a very general case. The one assumption we have to make is that for large z the potential is well-approximated by a constant (which was clearly the case in the concrete 5D model investigated above). This discussion is presented in appendix B.

While the wave function and spectral density for general μ^2 cannot be analytically determined, we can nonetheless solve the Schrödinger equation numerically (with the outgoing wave boundary conditions). It can be done either in the z or y coordinates (for the latter case the outgoing BC should be imposed very close to the singularity $y \rightarrow y_s$). This confirms the expression of the spectral density around the gap in eq. (6.24), which is illustrated in Fig. 4. In Fig. 5 we show the entire spectral density function obtained from numerically solving the Schrödinger equation.

As explained in section 3, the overall normalization of the spectral density is fixed by

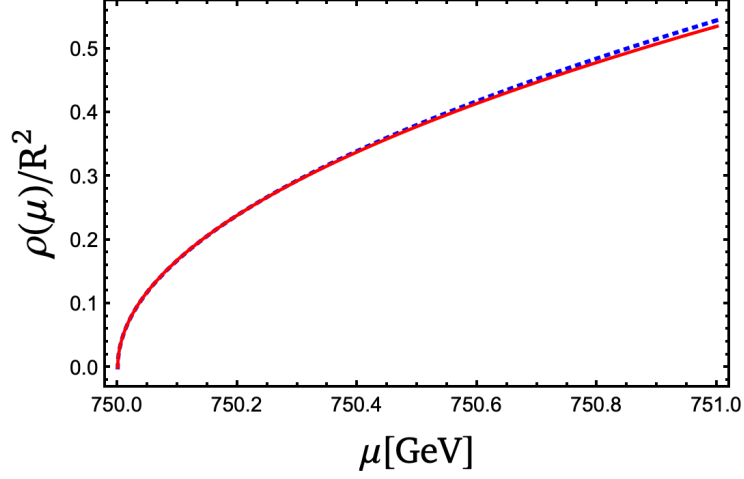


Figure 4. The shape of the spectral density near the gap scale μ_0 . For this plot, we choose $\mu_0 = 750$ GeV. The red solid curve is from the exact numerical solution and the blue dashed curve is a fit by a function $\rho(\mu^2) = \rho_0/\mu_0^2 (\mu^2/\mu_0^2 - 1)^{1/2}$ with a dimensionless normalization parameter ρ_0 .

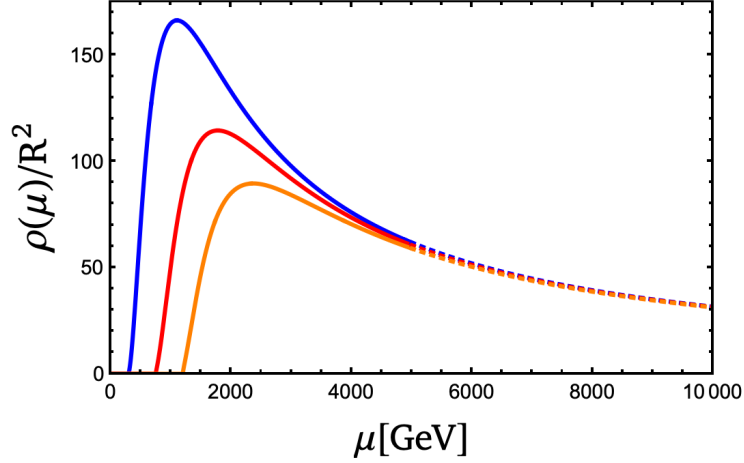


Figure 5. In this plot, we show the numerically obtained spectral density function over the full energy range assuming mass gaps: $\mu_0 = 300$ (Blue), 750 (Red), and 1200 (Orange) GeV. Below the cutoff of order \mathcal{O} (TeV), we show $\rho(\mu)$ in solid curves, while above the cutoff they are shown as dashed curves. As usual, ρ above the cutoff is not supposed to be used in effective theory calculations. Nevertheless, it is instructive to observe that ρ exhibits universal behavior, i.e. that of CFT.

the condition

$$\int_{\mu_0^2}^{\Lambda^2} \frac{d\mu^2}{2\pi} \rho(\mu^2) = 1. \quad (6.25)$$

Given a numerical solution of the Schrödinger equation, the normalization condition fixes

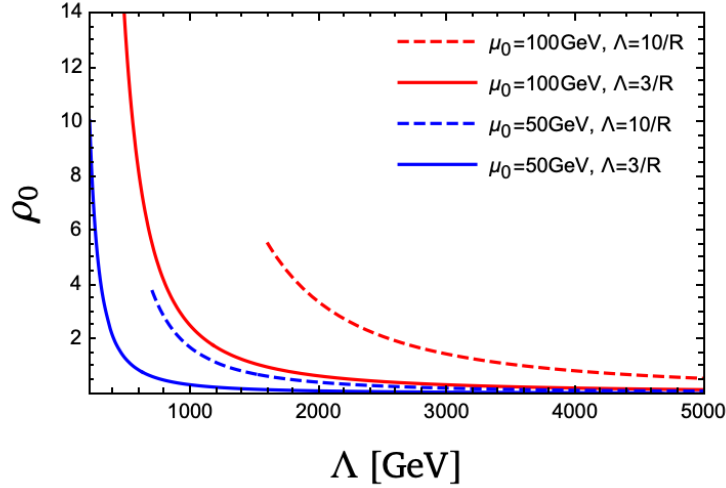


Figure 6. In this plot, we show the numerically obtained spectral density normalization ρ_0 as a function of the cutoff scale, with $\Lambda = \frac{3}{R}$ (solid), $\frac{10}{R}$ (dashed) and the mass gap at $\mu_0 = 50$ (Blue) and 100 (Red) GeV. Note that the spectral density is properly normalized taking the cutoff scale into account.

the value of ρ_0 in eq. (6.24). This value is important for many phenomenological predictions of the model, such as direct detection rates. An example is shown in fig. 6. We conclude that generally $\rho_0 \sim \mathcal{O}(1)$, but it does depend on the model parameters such as the location of the UV brane R and the cutoff scale Λ relative to $1/R$.

6.3 5D Z-portal Model

We are now ready to present the full 5D construction that incorporates the interactions of the continuum DM with the W and Z . We start with the same setup as in previous section 6.1 and section 6.2 and assume the background as in eq. (6.6) and eq. (6.7). The SM is localized on the UV brane. The action for the scalar dark matter Φ reads

$$S = S_{\text{bulk}} + S_{\text{UV}} \quad (6.26)$$

$$S_{\text{bulk}} = \int d^4x dy \sqrt{g} \left(g^{MN} (\partial_M \Phi)^\dagger (\partial_N \Phi) - m^2 |\Phi|^2 \right) \quad (6.27)$$

$$S_{\text{UV}} = \int_{\text{UV}} d^4x \left(\mathcal{L}_{\text{SM}} + |D_\mu \chi|^2 - m_\chi^2 |\chi|^2 - \hat{\lambda} \Phi \chi H + \text{h.c.} \right). \quad (6.28)$$

As explained below eq. (6.8) in section 6.2, using integration by parts, the bulk action can be rewritten so that the integrand is proportional to EoM of Φ , but with an extra boundary term induced on the UV brane given in eq. (6.9). Also, as shown in eqs. (6.12) and (6.17) the bulk EoM takes the form of a standard Schrödinger equation in terms of a new variable $\psi = e^{-\frac{3}{2}A} \Phi$ and conformal coordinate z related to y via $dz/dy = e^A$. The potential eq. (6.14) approaches a constant value at large z , see eq. (6.15), revealing that the spectrum consists of a continuum starting at the gap scale μ_0 . Once the solution for the “profile” $f(z, p)$ is found, we can integrate out the bulk by substituting f back into the

action. The bulk action vanishes trivially since it is directly proportional to the EoM. As a result, we obtain the boundary (or holographic) effective action (see also eq. (6.16)).

$$S_{\text{eff}} = \int \frac{d^4 p}{(2\pi)^4} \frac{1}{R} e^{\frac{5}{2}A(R)} \hat{\Phi}^\dagger(p) \partial_z \left(e^{\frac{3}{2}A(z)} \frac{f(z, p)}{f(R, p)} \right)_{z=R} \hat{\Phi}(p) + \int d^4 x \left(\mathcal{L}_{\text{SM}} + |D_\mu \chi|^2 - m_\chi^2 |\chi|^2 - \hat{\lambda} R^{-1/2} \hat{\Phi} \chi H + \text{h.c.} \right) \quad (6.29)$$

where the quadratic action of $\hat{\Phi}$ is expressed in momentum space since it is non-analytic in general. The reader may notice that this effective action is literally identical to our 4D effective model eq. (5.1) with simple identifications,

$$\Sigma(p^2) = \frac{C}{R} e^{\frac{5}{2}A(R)} \partial_z \left(e^{\frac{3}{2}A(z)} \frac{f(z, p)}{f(R, p)} \right)_{z=R} \quad (6.30)$$

$$\lambda = R^{-1/2} \hat{\lambda}.$$

The constant C is chosen to make $\hat{\Phi}$ canonically normalized (i.e. it satisfies the equal-time commutation relation). Here, we started with a local and unitary microscopic theory in 5D, which predicts a specific form of $\Sigma(p^2)$ as given in eq. (6.30). While the explicit form of the spectral density for arbitrary p^2 is not easy to work out analytically, nonetheless it is straightforward to find it numerically. Moreover, importantly, the form of the spectral density near the gap scale μ_0 takes a universal form, eq. (6.24), as shown in section 6.2 through an explicit 5D calculation. We also provide a more general argument in appendix B.

The couplings of the DM modes with the SM weak and hyper-charge gauge bosons needed to study phenomenology can be obtained as described in section 5. The final results are simply eq. (5.7) and eq. (5.8). The dependence on $\rho(\mu^2)$ comes in when we compute rates using the formalism presented in section 3.

7 Conclusion and Outlook

We presented a novel type of DM model, where the role of the dark sector is played by a Weakly Interacting Continuum (WIC). The continuum is assumed to be gapped at the weak scale, and interact with the SM EW sector, producing a continuum version of standard WIMP models. The continuum kinematics ensures that direct detection processes are strongly suppressed compared to familiar WIMPs, while in many other respects (relic abundance, indirect detection and some of the collider bounds) WIC DM is very similar to WIMPs. The suppression of the direct detection bounds re-opens the possibility of viable Z-portal DM models. A unique distinguishing aspect of WIC DM is the appearance of late decays of the sort $\text{DM}(\mu_1) \rightarrow \text{DM}(\mu_2) + \text{SM}$. Bounds on these late decays provide a lower bound on the interaction strength, leading to a well-defined allowed band in the parameter space. In addition, the WIC model has unique collider signatures driven by cascade decays of the continuum DM states produced at a collider.

In this paper we have focused on providing the details of the underlying construction both of the continuum itself as well as its interactions with the SM. We have carefully defined

the structure of generic free continuum field theories, which are subsequently coupled to the EW sector of the SM. We presented the structure of the Hilbert space for the free continuum and the basic elements of thermodynamics involving such states, which allowed us to derive the appropriate Boltzmann equation. We showed how to couple the continuum to the EW sector of the SM via a Higgs induced mixing. Using a simple effective theory of the continuum, we were able to calculate the relic density from the freeze-out of the WIC. A complete realistic model was obtained by considering a scalar field in a soft wall background in warped extra dimensions. This allowed us to find a concrete expression for the spectral density of a gapped continuum in a fully self-consistent theory, and verify the general form of the spectral density around the gap. The actual coupling to the SM is induced on the UV brane, providing a full implementation of the effective theory examined earlier. The full analysis of the phenomenology of this model will be presented in the companion paper [43].

In summary, we showed that a dark sector described by a gapped continuum QFT can provide a fully realistic dark matter candidate, with unique phenomenological features qualitatively different from any particle DM model. This opens up a new direction in DM model-building. While here we focused on weak-scale DM with a Z-portal, the idea can be applied to many other contexts, such as axionic DM, light thermal relics at the keV-GeV scales such as SIMPs, and so on. We look forward to further exploration in this direction.

Acknowledgments

We are grateful to Barry McCoy, Eun-Gook Moon, Carlos Wagner, Liantao Wang and Kathryn Zurek for helpful discussions. C.C., S.H. G.K. and M.P. were supported in part by the NSF grant PHY-2014071. C.C. was also supported in part by the US-Israeli BSF grant 2016153. S.H. was also supported by the DOE grants DE-SC-0013642 and DE-AC02-06CH11357 as well as a Hans Bethe Post-doctoral fellowship at Cornell. G.K. is supported by the Science and Technology Facilities Council with Grant No. ST/T000864/1. S.L. was supported by the Samsung Science & Technology Foundation. W.X. was supported in part by the DOE grant DE-SC0010296.

A Gapped Continuum from Five-Dimensional Flat Space

In this appendix we consider an infinite, flat 5D space with coordinates (x^μ, z) . A 5D scalar field $\Phi(x^\mu, z)$ with mass m_0 propagates on this space. We discuss how this theory can be alternatively described as a 4D theory with a gapped continuum spectrum. We should note that this setup cannot be used to construct realistic models of the kind we consider in the paper, because gravity remains five-dimensional at all distance scales. Still, it is a useful example to consider to gain intuition about gapped continuum spectrum and spectral density in a simple context.

A.1 Infinite 5D and Spectral Density

The scalar propagator has the form

$$\langle \Phi(x^\mu, z) \Phi(0) \rangle = \int \frac{d^5 P}{(2\pi)^5} \frac{i}{P^2 - m_0^2 + i\epsilon} e^{-i(p \cdot x - zk)}, \quad (\text{A.1})$$

where $P = (p^\mu, k)$. Fourier transforming into momentum space along the four x^μ dimensions, we get

$$\Pi(p^2, z) = \int \frac{dk}{2\pi} \frac{i}{p^2 - (k^2 + m_0^2) + i\epsilon} e^{izk}. \quad (\text{A.2})$$

Consider a 4D “brane” at $z = 0$. The brane-to-brane propagator is

$$\Pi(p^2, 0) = \int \frac{dk}{2\pi} \frac{i}{p^2 - (k^2 + m_0^2) + i\epsilon}. \quad (\text{A.3})$$

Defining $s = k^2 + m_0^2$, we can rewrite

$$\Pi(p^2, 0) = \int_{m_0^2}^{+\infty} \frac{ds}{2\pi} \frac{i}{p^2 - s + i\epsilon} \rho(s), \quad (\text{A.4})$$

where

$$\rho(s) = \frac{1}{2\sqrt{s - m_0^2}} \quad (\text{A.5})$$

is the spectral density. Thus we have recast this trivial 5D theory as a 4D theory with gapped continuum spectrum and a non-trivial spectral density.

A.2 Compactified Theory and KK Picture

Let us now consider the same theory with the z direction compactified on a circle of radius R . This gives a familiar KK theory. The scalar field decomposes as $\Phi(x, z) = \sum_n f_n(z) \phi_n(x)$, where $\phi_n(x)$ are 4D fields with masses

$$m_n^2 = m_0^2 + \left(\frac{n}{R}\right)^2. \quad (\text{A.6})$$

and $f_n = \frac{1}{\sqrt{2\pi R}} \cos(n\pi z/R)$. The brane-to-brane propagator can then be expressed as

$$\langle \Phi(x^\mu, 0) \Phi(0) \rangle = \sum_{m,n} f_n(0) f_m(0) \langle \phi_n(x) \phi_m(0) \rangle, \quad (\text{A.7})$$

which gives

$$\Pi(p^2, 0) = \frac{1}{2\pi R} \sum_n \frac{i}{p^2 - m_n^2 + i\epsilon}. \quad (\text{A.8})$$

Now consider going back to the infinite 5D theory by taking the limit $R \rightarrow \infty$. We expect that in this limit the sum over n turns into an integral over KK mass, labeled by a continuum

parameter μ^2 . For large R , the splitting between neighboring KK modes is

$$\Delta\mu_n^2 \equiv m_{n+1}^2 - m_n^2 \approx \frac{2n}{R^2} = \frac{2}{R} \sqrt{\mu^2 - m_0^2}. \quad (\text{A.9})$$

Thus,

$$\sum_n = \sum_n \frac{\Delta\mu_n^2}{\Delta\mu_n^2} \rightarrow \int_{m_0^2}^{\infty} d\mu^2 (R/2) \frac{1}{\sqrt{\mu^2 - m_0^2}} = \int_{m_0^2}^{\infty} d\mu^2 R \rho(\mu^2), \quad (\text{A.10})$$

where ρ is the spectral density function given in Eq. (A.5). Plugging into Eq. (A.8)

$$\Pi(p^2, 0) = \int_{m_0^2}^{\infty} \frac{d\mu^2}{2\pi} \frac{i}{p^2 - \mu^2 + i\epsilon} \rho(\mu^2). \quad (\text{A.11})$$

This is exactly the same spectral-density representation of the brane-to-brane propagator as in Eq. (B.10). This derivation makes it explicit that the physical meaning of the spectral density $\rho(\mu^2)$ is (up to an overall constant) the density of KK states with respect to μ^2 .

A.3 Hilbert Space, Orthonormality and Completeness

The one-particle Hilbert space of our theory in infinite 5D is spanned by basis states $|\mathbf{p}, k\rangle$. These are eigenstates of 5D momentum, with eigenvalues given by $(E_{\mathbf{p}, \mathbf{k}}, \mathbf{p}, k)$ where $E_{\mathbf{p}, \mathbf{k}} = \sqrt{\mathbf{p}^2 + k^2 + m_0^2}$. These states obey orthonormality and completeness relations:

$$\begin{aligned} \int \frac{d^3p}{(2\pi)^3} \frac{dk}{2\pi} \frac{1}{2E_{\mathbf{p}, \mathbf{k}}} |\mathbf{p}, k\rangle \langle \mathbf{p}, k| &= 1, \\ \langle \mathbf{p}', k' | \mathbf{p}, k \rangle &= (2\pi)^4 (2E_{\mathbf{p}, \mathbf{k}}) \delta^3(\mathbf{p}' - \mathbf{p}) \delta(k' - k). \end{aligned} \quad (\text{A.12})$$

The factors of energy are a matter of convention; with our choice the scalar product of basis states is Lorentz-invariant.

Now, let us define $\mu^2 \equiv k^2 + m_0^2$. We can choose to label our basis states by μ^2 instead of k : $|\mathbf{p}, \mu^2\rangle \equiv |\mathbf{p}, k = \sqrt{\mu^2 - m_0^2}\rangle$. Note that

$$\frac{d\mu^2}{dk} = 2k = 2\sqrt{\mu^2 - m_0^2} = \frac{1}{\rho(\mu^2)}. \quad (\text{A.13})$$

Using this Jacobean, the orthonormality and completeness relations become

$$\begin{aligned} \int \frac{d^3p}{(2\pi)^3} \frac{d\mu^2}{2\pi} \frac{1}{2E_{\mathbf{p}, \mu^2}} \rho(\mu^2) |\mathbf{p}, \mu^2\rangle \langle \mathbf{p}, \mu^2| &= 1, \\ \langle \mathbf{p}', \mu'^2 | \mathbf{p}, \mu^2 \rangle &= (2\pi)^4 \frac{2E_{\mathbf{p}, \mu^2}}{\rho(\mu^2)} \delta^3(\mathbf{p}' - \mathbf{p}) \delta(\mu'^2 - \mu^2), \end{aligned} \quad (\text{A.14})$$

where $E_{\mathbf{p}, \mu^2} = \sqrt{\mathbf{p}^2 + \mu^2}$. This is precisely the formulas given in the main text (see eq. (3.13) and (eq. (3.15))).

An alternative derivation of this result is to start with a compactified 5D space, where the one-particle states are the usual KK modes $|\mathbf{p}, n\rangle$. These obey the orthonormality and

completeness relations

$$\begin{aligned} \sum_n \int \frac{d^3 p}{(2\pi)^3} \frac{1}{2E_{\mathbf{p},n}} |\mathbf{p}, n\rangle \langle \mathbf{p}, n| &= 1, \\ \langle \mathbf{p}', n' | \mathbf{p}, n \rangle &= (2\pi)^3 (2E_{\mathbf{p},n}) \delta_{nn'} \delta^3(\mathbf{p}' - \mathbf{p}). \end{aligned} \quad (\text{A.15})$$

Here $E_{\mathbf{p},n} = \sqrt{\mathbf{p}^2 + m_n^2}$. The continuum limit in the completeness relation is obtained by replacing

$$\sum_n \rightarrow R \int d\mu^2 \rho(\mu^2), \quad (\text{A.16})$$

as in Eq. (A.10) above. In the orthonormality relation, this continuum limit is taken using

$$\delta_{n,n'} \rightarrow \frac{1}{R \rho(\mu^2)} \delta(\mu'^2 - \mu^2). \quad (\text{A.17})$$

Rescaling the one-particle states to define

$$|\mathbf{p}, \mu^2\rangle \equiv \lim_{R \rightarrow \infty} \sqrt{R} \left| \mathbf{p}, n = R\sqrt{\mu^2 - \mu_0^2} \right\rangle, \quad (\text{A.18})$$

we again reproduce the orthonormality and completeness relations used in the main text.

A.4 Boltzmann Equation

The 5D flat-space model also gives a useful illustration of Boltzmann equations for gapped continuum. A gas of single-particle excitations in this model can be described by a 5D phase-space distribution $f(\mathbf{p}, k)$. To add interactions, let us consider a toy model where the 5D field Φ is coupled to a 4D field $h(x)$ localized on a brane at $z = 0$, via

$$S_{\text{int}} = \int d^4 x \frac{\lambda}{4} \Phi^2 h^2. \quad (\text{A.19})$$

This interaction enables a $2 \rightarrow 2$ scattering processes $\Phi\Phi \leftrightarrow hh$. Notice that 4D momentum is conserved in this scattering, but 5D momentum is not, due to the localized nature of the interaction. The standard textbook derivation of the Boltzmann equation trivially generalizes to the flat 5D space, yielding¹⁴

$$\begin{aligned} E \frac{\partial f(\mathbf{p}, k, t)}{\partial t} &= -\frac{1}{2} \int d\Pi'^{(5)} d\Pi_A d\Pi_B (2\pi)^4 \delta^4(q_A + q_B - p - p') \\ &\times |\mathcal{M}|^2 (ff'(1 \pm f_A)(1 \pm f_B) - f_A f_B (1 \pm f)(1 \pm f')). \end{aligned} \quad (\text{A.20})$$

In the collision term on the right-hand side, q_A and q_B denote the 4-momenta of the h particles in the collision, while $P = (p^\mu, k)$ and $P' = (p'^\mu, k')$ are the 5-momenta of the Φ particles. Once again, only the 4-momentum is conserved, as reflected in the delta function

¹⁴This form of the Boltzmann equation would apply for any interaction between two 5D fields and two fields localized on a 4D delta-function brane. For example, h can be replaced by a particle with spin.

in the collision term. The LIPS volume elements for the 4D h particles take their usual form, $d\Pi_{A,B} \equiv \frac{d^3 q_{A,B}}{(2\pi)^3} \frac{1}{2E_{A,B}}$, while the LIPS volume element for the 5D Φ particle with momentum P' has the form

$$d\Pi'^{(5)} \equiv \frac{dk'}{2\pi} \frac{d^3 p'}{(2\pi)^3} \frac{1}{2E'} = \frac{dk'}{2\pi} d\Pi_{\mu'}, \quad (\text{A.21})$$

where $E' = \sqrt{\mathbf{p}'^2 + k'^2 + m_0^2}$ is the particle's energy, and in the second equality $d\Pi_{\mu'}$ is the usual LIPS volume element for a 4D particle with 3-momentum \mathbf{p}' and mass $\mu' = \sqrt{k'^2 + m_0^2}$. Changing the integration variable from k' to μ'^2 yields

$$E \frac{\partial f(\mathbf{p}, k, t)}{\partial t} = -\frac{1}{2} \int \frac{d\mu'^2}{2\pi} \rho(\mu'^2) \int d\Pi_{\mu'} d\Pi_A d\Pi_B (2\pi)^4 \delta^4(q_A + q_B - p - p') \\ \times |\mathcal{M}|^2 (ff'(1 \pm f_A)(1 \pm f_B) - f_A f_B (1 \pm f)(1 \pm f')), \quad (\text{A.22})$$

where once again the spectral density ρ arises as the Jacobean of the variable change. This is precisely Eq. (3.27) which formed the basis of our discussion of non-equilibrium thermodynamics in section 3 and section 4.

B Spectral Density Near the Gap

As we discussed in section 1 and section 2, most of the continuum DM phenomenology is governed by the shape of the spectral density near the gap scale. In section 6 we presented the expression for the spectral density near the mass gap eq. (6.24) for the particular background geometry of eq. (6.6) and eq. (6.7). Here we would like to argue that the characteristic square root form obtained is quite general, and applicable to any case with a gapped continuum described by the Schrödinger equation

$$-\frac{d^2 \psi}{dz^2} + V(z)\psi = \kappa^2 \psi. \quad (\text{B.1})$$

where $\kappa^2 = p^2 - \mu_0^2$ is the distance from the gap while as before μ_0 is the gap scale. We assume that $V(z)$ is positive-definite and $V \rightarrow 0$ as $z \rightarrow +\infty$ (the constant corresponding to the gap is already included in the definition of κ^2). This equation is guaranteed to have two *real*, linearly-independent solutions ψ_1 and ψ_2 . The general solution (up to an irrelevant overall constant) is¹⁵

$$\psi = \psi_1 + c\psi_2, \quad (\text{B.2})$$

where c can be complex. At large z , V can be ignored and the equation can be solved:

$$\psi_1 = \cos \kappa z, \quad \psi_2 = \sin \kappa z. \quad (\text{B.3})$$

The outgoing wave boundary condition at $z \rightarrow +\infty$ is $\psi \sim e^{+i\kappa z}$, which fixes $c = i$.

¹⁵In fact, the overall factor is in general a function of p^2 . This however cancels out in $\Sigma(p)$, and hence in $\rho(p^2)$.

We recall that the spectral density is given by

$$\rho(p^2) = -2\text{Im}\frac{1}{\Sigma(p)} = -2\frac{\text{Im}\bar{\Sigma}(p)}{|\Sigma(p)|^2} \quad (\text{B.4})$$

where $\Sigma(p) = k\partial_z \left(e^{\frac{3}{2}A(z)} \frac{\psi(z,p)}{\psi(R,p)} \right)_{z=R}$ ¹⁶ and $\bar{\Sigma}$ is the complex conjugate of Σ . Obviously, $\text{Im}\bar{\Sigma} = -\text{Im}\Sigma$. Explicit computation shows that

$$\rho(p^2) = 2\frac{\text{Im}\Sigma(p)}{k} \left[\left(\frac{3}{2}(k + 1/y_s) + \frac{\text{Re}(\bar{\psi}\psi')}{|\psi|^2} \right)_{z=R}^2 + (\text{Im}\Sigma)^2 \right]^{-1} \quad (\text{B.5})$$

where we remind that k is AdS curvature scale (while $\kappa = \sqrt{p^2 - \mu_0^2}$). The point of this expression is that the behavior of $\rho(p^2)$ at the gap scale $p^2 \rightarrow \mu_0^2$ is understood from that of $\text{Im}\Sigma$. Also, relatedly, the regularity (or singularity) is determined by how $|\psi|^2$ behaves at $z = R$, the UV-brane scale. For this reason, from now on, we focus on (note that $A(z)$ is a real function)

$$\text{Im}\Sigma(p) = k \text{Im} \left. \frac{d}{dz} \log \psi \right|_{z=R}. \quad (\text{B.6})$$

The log-derivative of the wavefunction is given by

$$\frac{d}{dz} \log \psi = \frac{\psi'_1 + i\psi'_2}{\psi_1 + i\psi_2} \quad (\text{B.7})$$

and its imaginary part (remembering that both ψ_i 's are real) is

$$\text{Im} \frac{d}{dz} \log \psi = \frac{\psi_1\psi'_2 - \psi'_1\psi_2}{|\psi_1|^2 + |\psi_2|^2}. \quad (\text{B.8})$$

The numerator is the Wronskian W . Since Eq. (B.1) has no first-derivative term, by the Abel identity W is a z -independent constant. We can compute W at large z using Eq. (B.3): $W = \kappa (\cos^2 \kappa z + \sin^2 \kappa z) = \kappa$. So we have

$$\text{Im} \frac{d}{dz} \log \psi = \frac{\kappa}{|\psi(z)|^2} = \frac{\sqrt{p^2 - \mu_0^2}}{|\psi(z)|^2}. \quad (\text{B.9})$$

This is valid at any z , in particular at the location of the UV brane. Therefore

$$\rho(p^2) \propto \frac{\sqrt{p^2 - \mu_0^2}}{|\psi(R)|^2}. \quad (\text{B.10})$$

This almost proves that $G(p^2) \rightarrow 0$ as $p^2 \rightarrow \mu_0^2$; the only caveat is that we still need to prove that $|\psi(R)| \neq 0$ in this limit. A simple argument is that since $z = R$ is arbitrary, and we cannot have $|\psi(R)| = 0$ for more than a finite set of values of $z = R$, generically

¹⁶In section 6 we denoted the profile as $f(z, p)$, which satisfies the same Schrödinger equation.

we should expect it to be non-zero. However a stronger argument can be constructed that in fact it *cannot* be 0. Multiply Eq. (B.1) on both sides by ψ^* , and integrate over z from some z_0 to $+\infty$. Then use integration by parts on the first term. This gives

$$-\left(\frac{d}{dz}|\psi|^2\right)\Big|_{z_0}^{+\infty} + \int_{z_0}^{+\infty} dz \left[|\psi'|^2 + V(z)|\psi|^2\right] = \kappa^2 \int_{z_0}^{+\infty} dz |\psi|^2. \quad (\text{B.11})$$

Dropping terms proportional to powers of κ (as $\kappa \rightarrow 0$ for modes $p^2 \rightarrow \mu_0^2$), we have

$$\frac{d}{dz}|\psi|^2(z_0) + \int_{z_0}^{+\infty} dz \left[|\psi'|^2 + V(z)|\psi|^2\right] = 0 \quad (\text{B.12})$$

which implies

$$\frac{d}{dz}|\psi|^2(z_0) < 0, \quad (\text{B.13})$$

for modes very close to the gap scale μ_0 . Since z_0 was arbitrary, this means that $|\psi|^2$ is a monotonically decreasing function, and since we know that $|\psi|^2 = 1$ at large positive z (see eq. (B.3)), it means that $|\psi|^2 \geq 1$ for any z and therefore non-zero at the UV-brane $z = R$.

One may still worry that the wave function itself is diverging at $z = R$, and hence strongly influencing the way the spectral density goes to zero at the gap. However, again $z = R$ is not a special point in the geometry, but in fact arbitrarily chosen, hence the potential or wave function is not expected to have a singularity at $z = R$. Therefore for the generic case, we expect that $\lim_{\kappa \rightarrow 0} |\psi(R)|^2 = C$, some *finite* constant. In this case according to eq. (B.10),

$$\rho(p^2) \propto \sqrt{p^2 - \mu_0^2}. \quad (\text{B.14})$$

One implication of this is that $\rho(p^2) \rightarrow 0$ as $p^2 \rightarrow \mu_0^2$. Notice also that as long as $\lim_{\kappa \rightarrow 0} |\psi(R)|^2 = C < \infty$, $\rho(p^2)$ is regular for p^2 close to μ_0^2 as is seen directly from appendix B. In fact, this is exactly what we have found in section 6 computed in the background, eq. (6.6) and eq. (6.7), both using the analytic asymptotic solution as well as the numerical solution. It may be worth mentioning that it is possible to solve the eq. (B.1) analytically for $V(z) \propto e^{-az}$ for any constant a and one finds that $\text{Im}\Sigma \propto \sqrt{p^2 - \mu_0^2}$. In section 6, we indeed have shown that the form of the potential at $z \rightarrow \infty$ do have this form with $a = \frac{2}{3}\mu_0$.

C AdS/CFT Duality of Gapped Continuum

In this appendix, we describe 4D CFT dual description of the 5D Z -portal model introduced in section 6.3. The boundary effective action $S_{\text{eff}}[\hat{\Phi}]$ derived in section 6.3 is interpreted as (the leading order in large- N expansion) partition function of the dual CFT via the

AdS/CFT correspondence [59–61]:

$$Z_{\text{AdS}}[\hat{\Phi}] = \int_{\text{AdS}} \mathcal{D}\Phi|_{\Phi|_{\text{UV}}=\hat{\Phi}} e^{iS_{\text{AdS}}[\Phi]} \approx e^{iS_{\text{eff}}[\hat{\Phi}]} \quad (\text{C.1})$$

$$= \int_{\text{CFT}} \mathcal{D}\varphi e^{iS_{\text{CFT}}[\varphi] + iS_{\text{ext}}[\hat{\Phi}] + i \int \frac{1}{\Lambda^{d-3}} \hat{\Phi}^\dagger \mathcal{O} + \text{h.c.}} = Z_{\text{CFT}}[\hat{\Phi}]. \quad (\text{C.2})$$

where d is the scaling dimension of the CFT operator \mathcal{O} sourced by the UV boundary value $\hat{\Phi}$ of 5D field Φ . With finite UV cutoff scale Λ , the source field $\hat{\Phi}$ may be dynamical, and for this reason we added the action $S_{\text{ext}}[\hat{\Phi}]$ for the external field $\hat{\Phi}$. From this, we can derive the relation between CFT two point function and $\Sigma(p^2)$

$$\Sigma(p^2) = \frac{i}{\Lambda^{2d-6}} \langle \mathcal{O} \mathcal{O}^\dagger \rangle(p) + G_{\hat{\Phi}}(p^2) \quad (\text{C.3})$$

where $G_{\hat{\Phi}}(p^2)$ is two point function of $\hat{\Phi}$ obtained from $S_{\text{ext}}[\hat{\Phi}]$, possibly including wave function renormalization factor. For instance, if $S_{\text{ext}}[\hat{\Phi}] = Z \partial_\mu \hat{\Phi}^\dagger \partial^\mu \hat{\Phi}$ then $G_{\hat{\Phi}}(p^2) = Z p^2$. In the IR, the dual 4D QFT goes through a phase transition into gapped continuum phase. In this phase, a CFT operator creates composite (gapped) continuum states and the source term $\hat{\Phi}^\dagger \mathcal{O}$ describes a mixing between external degree of freedom $\hat{\Phi}$ and composite continuum modes. To understand this mixing better, we may write the CFT operator in terms of canonically normalized field $\phi_\mu(x)$ which excites a mode with $p^2 = \mu^2$ as

$$\mathcal{O}(x) = \mu_0^{d-1} \int_1^\infty \frac{d(\mu/\mu_0)}{2\pi} c(\mu/\mu_0) \phi_\mu(x). \quad (\text{C.4})$$

Here, μ_0 is the gap scale and the dimensionless function $c(\mu/\mu_0)$ has a support from μ_0 to some $\mu \sim \mathcal{O}(\Lambda)$, hence determines the integration upper limit. As we show below, this function is directly related to the spectral density. Using

$$\langle \phi_\mu^\dagger(p) \phi_{\mu'}(k) \rangle = \frac{i}{p^2 - \mu^2 + i\epsilon} (2\pi)^4 \delta^4(p - k) (2\pi) \delta\left(\frac{\mu}{\mu_0} - \frac{\mu'}{\mu_0}\right) \quad (\text{C.5})$$

we can rewrite the continuum part in appendix C as

$$\Sigma_c(p^2) \equiv \Sigma(p^2) - G_{\hat{\Phi}}(p^2) = \frac{\mu_0^{2d-3}}{\Lambda^{2d-6}} \int_{\mu_0^2}^\infty \frac{d\mu^2}{2\pi} \frac{[c(\mu/\mu_0)^2/2\mu]}{\mu^2 - p^2 - i\epsilon}. \quad (\text{C.6})$$

This in turn implies that

$$\text{Im}\Sigma_c(p^2) = \frac{\mu_0^{2d-3}}{\Lambda^{2d-6}} \left[c(p/\mu_0)^2/4p \right], \quad p = \sqrt{p^2}. \quad (\text{C.7})$$

In addition, the mixing between the external field and the composite continuum modes is readily found to be

$$\mathcal{L} \supset \frac{1}{\Lambda^{d-3}} \hat{\Phi}^\dagger \mathcal{O} = \int \frac{d(\mu/\mu_0)}{2\pi} \sqrt{4\mu_0\mu \text{Im}\Sigma_c} \hat{\Phi}^\dagger \phi_\mu \quad (\text{C.8})$$

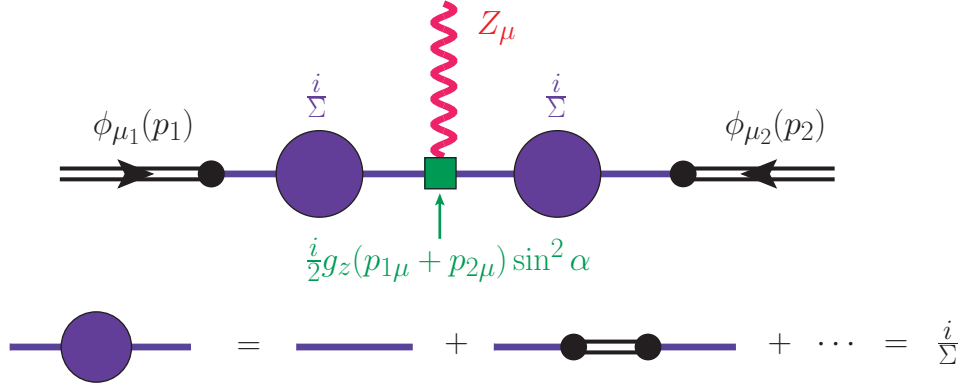


Figure 7. Effective coupling in CFT picture through the resummation of $\hat{\Phi}$ – ϕ_μ mixing. Composite continuum modes ϕ_μ are denoted as double lines and the external field $\hat{\Phi}$ is depicted with a single line.

where we used appendix C to get the final expression.

In the CFT picture, it is the external field $\hat{\Phi}$ that couples to the SM Z and W . Then the coupling of continuum modes to the Z and W is obtained through mixing. One thing that we need to be a bit careful is that we need to resum all the diagrams to get reliable answer, since the μ -dependent mixing given in appendix C is generally not small. This may be done by first computing resummed $\hat{\Phi}$ -propagator and inserting such resummed propagator into the relevant Feynman diagrams. It is straightforward to show that the resummation of the diagrams in fig. 7 yields

$$\langle \hat{\Phi} \hat{\Phi}^\dagger \rangle(p) = \frac{i}{G_{\hat{\Phi}}} + \frac{i}{G_{\hat{\Phi}}} \left(\frac{i}{\Lambda^{d-3}} \right)^2 \langle \mathcal{O} \mathcal{O}^\dagger \rangle \frac{i}{G_{\hat{\Phi}}} + \dots = \frac{i}{G_{\hat{\Phi}} + i \frac{1}{\Lambda^{2d-6}} \langle \mathcal{O} \mathcal{O}^\dagger \rangle} = \frac{i}{\Sigma(p^2)}. \quad (\text{C.9})$$

In fact, we could have obtained this easily from holographic effective action by viewing it as an action for $\hat{\Phi}$ including CFT contributions (i.e. resummation). Then the coupling of a pair of continuum modes (μ_1 and μ_2) to the Z boson is given by

$$g_{\text{eff}} = \left[\frac{i}{2} g (p_1 + p_2)_\mu \right] \left[\sin \alpha_{\mu_1} \sqrt{2\mu_0 \mu_1 \rho(\mu_1^2)} \right] \left[\sin \alpha_{\mu_2} \sqrt{2\mu_0 \mu_2 \rho(\mu_2^2)} \right]. \quad (\text{C.10})$$

To get this, we used

$$\rho(\mu^2) = -2\text{Im}\Sigma^{-1} = 2 \frac{\text{Im}\Sigma_c}{|\Sigma|^2} \quad (\text{C.11})$$

and appendix C. Note that $\text{Im}\Sigma = \text{Im}\Sigma_c$. We also remind that the first factor is the usual coupling to Z -boson, and $\sin \alpha_\mu$ is from the mixing $\hat{\Phi}$ with χ that directly couples to Z (see section 5). Therefore, we see that the effective coupling is a product of the usual Z -coupling of a complex scalar (the first factor) and mixing angle for each continuum modes (the second and third factors).

Finally, let us compute the cross section for a process in which two SM particles A and B annihilate into a pair of continuum DM with μ_1 and μ_2 through the Z -exchange. For concreteness, let us assume (as we did so far) that $\sin \alpha_\mu$ is μ -independent, which may be achieved by taking $m_\chi \gg \mu$. Denoting $\delta_\mu \equiv \sqrt{2\mu_0\mu\rho(\mu^2)}$, the matrix amplitude may be written as

$$\mathcal{M}(A+B \rightarrow \text{DM}(\mu_1) + \text{DM}(\mu_2)) = \delta_{\mu_1}\delta_{\mu_2}\hat{\mathcal{M}} \quad (\text{C.12})$$

where we factored out the entire μ -dependent piece in the form of mixing angles, and defined the μ -independent matrix element $\hat{\mathcal{M}}$ which is just a matrix element for particles with mass μ_1 and μ_2 . The cross section with the possible final states summed over (at the level of rate, not the matrix element) then is given by

$$\sigma(A+B \rightarrow \text{DM}(\mu_1) + \text{DM}(\mu_2)) = \int \frac{d\mu_1^2}{2\pi} \rho(\mu_1^2) \int \frac{d\mu_2^2}{2\pi} \rho(\mu_2^2) \hat{\sigma} \quad (\text{C.13})$$

where similarly to the matrix element, $\hat{\sigma}$ is a cross section computed in terms of $\hat{\mathcal{M}}$ in a way that continuum modes are treated as particles with mass μ_1^2 and μ_2^2 . Clearly then, the phase space density for these canonically normalized continuum modes are the usual Lorentz invariant measure given in eq. (3.18). Crucially, this final expression, obtained with mixing angles and proper mode-sum defined through appendix C, agrees exactly with eq. (3.17).

References

- [1] G. Bertone and D. Hooper, “History of dark matter,” *Rev. Mod. Phys.* **90** no. 4, (2018) 045002, [arXiv:1605.04909 \[astro-ph.CO\]](#).
- [2] J. Silk *et al.*, *Particle Dark Matter: Observations, Models and Searches*. Cambridge Univ. Press, Cambridge, 2010.
- [3] L. Bergstrom, “Dark Matter Candidates,” *New J. Phys.* **11** (2009) 105006, [arXiv:0903.4849 \[hep-ph\]](#).
- [4] J. L. Feng, “Dark Matter Candidates from Particle Physics and Methods of Detection,” *Ann. Rev. Astron. Astrophys.* **48** (2010) 495–545, [arXiv:1003.0904 \[astro-ph.CO\]](#).
- [5] J. M. Gaskins, “A review of indirect searches for particle dark matter,” *Contemporary Physics* **57** no. 4, (2016) 496–525.
- [6] M. Schumann, “Direct Detection of WIMP Dark Matter: Concepts and Status,” *J. Phys. G* **46** no. 10, (2019) 103003, [arXiv:1903.03026 \[astro-ph.CO\]](#).
- [7] F. Kahlhoefer, “Review of LHC Dark Matter Searches,” *Int. J. Mod. Phys. A* **32** no. 13, (2017) 1730006, [arXiv:1702.02430 \[hep-ph\]](#).
- [8] M. Frigerio, A. Pomarol, F. Riva, and A. Urbano, “Composite Scalar Dark Matter,” *JHEP* **07** (2012) 015, [arXiv:1204.2808 \[hep-ph\]](#).
- [9] J. M. Cline, Z. Liu, G. Moore, and W. Xue, “Composite strongly interacting dark matter,” *Phys. Rev. D* **90** no. 1, (2014) 015023, [arXiv:1312.3325 \[hep-ph\]](#).

- [10] A. Kusenko and M. E. Shaposhnikov, “Supersymmetric Q balls as dark matter,” *Phys. Lett. B* **418** (1998) 46–54, [arXiv:hep-ph/9709492](#).
- [11] S. Hawking, “Gravitationally collapsed objects of very low mass,” *Mon. Not. Roy. Astron. Soc.* **152** (1971) 75.
- [12] B. Carr, F. Kuhnel, and M. Sandstad, “Primordial Black Holes as Dark Matter,” *Phys. Rev. D* **94** no. 8, (2016) 083504, [arXiv:1607.06077 \[astro-ph.CO\]](#).
- [13] M. Sasaki, T. Suyama, T. Tanaka, and S. Yokoyama, “Primordial black holes—perspectives in gravitational wave astronomy,” *Class. Quant. Grav.* **35** no. 6, (2018) 063001, [arXiv:1801.05235 \[astro-ph.CO\]](#).
- [14] C. J. Hogan and M. J. Rees, “AXION MINICLUSTERS,” *Phys. Lett. B* **205** (1988) 228–230.
- [15] E. W. Kolb and I. I. Tkachev, “Axion miniclusters and Bose stars,” *Phys. Rev. Lett.* **71** (1993) 3051–3054, [arXiv:hep-ph/9303313](#).
- [16] E. W. Kolb and I. I. Tkachev, “Nonlinear axion dynamics and formation of cosmological pseudosolitons,” *Phys. Rev. D* **49** (1994) 5040–5051, [arXiv:astro-ph/9311037](#).
- [17] K. M. Zurek, C. J. Hogan, and T. R. Quinn, “Astrophysical Effects of Scalar Dark Matter Miniclusters,” *Phys. Rev. D* **75** (2007) 043511, [arXiv:astro-ph/0607341](#).
- [18] E. Hardy, “Miniclusters in the Axiverse,” *JHEP* **02** (2017) 046, [arXiv:1609.00208 \[hep-ph\]](#).
- [19] K. R. Dienes and B. Thomas, “Dynamical Dark Matter: I. Theoretical Overview,” *Phys. Rev. D* **85** (2012) 083523, [arXiv:1106.4546 \[hep-ph\]](#).
- [20] K. R. Dienes and B. Thomas, “Dynamical Dark Matter: II. An Explicit Model,” *Phys. Rev. D* **85** (2012) 083524, [arXiv:1107.0721 \[hep-ph\]](#).
- [21] A. Katz, M. Reece, and A. Sajjad, “Continuum-mediated dark matter–baryon scattering,” *Phys. Dark Univ.* **12** (2016) 24–36, [arXiv:1509.03628 \[hep-ph\]](#).
- [22] I. Chaffey, S. Fichet, and P. Tanedo, “Continuum-Mediated Self-Interacting Dark Matter,” [arXiv:2102.05674 \[hep-ph\]](#).
- [23] **XENON** Collaboration, E. Aprile *et al.*, “Dark Matter Search Results from a One Ton-Year Exposure of XENON1T,” *Phys. Rev. Lett.* **121** no. 11, (2018) 111302, [arXiv:1805.12562 \[astro-ph.CO\]](#).
- [24] **PandaX-II** Collaboration, X. Cui *et al.*, “Dark Matter Results From 54-Ton-Day Exposure of PandaX-II Experiment,” *Phys. Rev. Lett.* **119** no. 18, (2017) 181302, [arXiv:1708.06917 \[astro-ph.CO\]](#).
- [25] **LUX** Collaboration, D. S. Akerib *et al.*, “Results from a search for dark matter in the complete LUX exposure,” *Phys. Rev. Lett.* **118** no. 2, (2017) 021303, [arXiv:1608.07648 \[astro-ph.CO\]](#).
- [26] M. Escudero, A. Berlin, D. Hooper, and M.-X. Lin, “Toward (Finally!) Ruling Out Z and Higgs Mediated Dark Matter Models,” *JCAP* **12** (2016) 029, [arXiv:1609.09079 \[hep-ph\]](#).
- [27] H. Georgi, “Unparticle physics,” *Phys. Rev. Lett.* **98** (2007) 221601, [arXiv:hep-ph/0703260](#).
- [28] B. Grinstein, K. A. Intriligator, and I. Z. Rothstein, “Comments on Unparticles,” *Phys. Lett. B* **662** (2008) 367–374, [arXiv:0801.1140 \[hep-ph\]](#).

- [29] S. S. Gubser, “Curvature singularities: The Good, the bad, and the naked,” *Adv. Theor. Math. Phys.* **4** (2000) 679–745, [arXiv:hep-th/0002160](#).
- [30] D. Z. Freedman, S. S. Gubser, K. Pilch, and N. P. Warner, “Continuous distributions of D3-branes and gauged supergravity,” *JHEP* **07** (2000) 038, [arXiv:hep-th/9906194](#).
- [31] P. Kraus, F. Larsen, and S. P. Trivedi, “The Coulomb branch of gauge theory from rotating branes,” *JHEP* **03** (1999) 003, [arXiv:hep-th/9811120](#).
- [32] J. A. Cabrer, G. von Gersdorff, and M. Quiros, “Soft-Wall Stabilization,” *New J. Phys.* **12** (2010) 075012, [arXiv:0907.5361 \[hep-ph\]](#).
- [33] B. Bellazzini, C. Csáki, J. Hubisz, S. J. Lee, J. Serra, and J. Terning, “Quantum Critical Higgs,” *Phys. Rev. X* **6** no. 4, (2016) 041050, [arXiv:1511.08218 \[hep-ph\]](#).
- [34] C. Csáki, G. Lee, S. J. Lee, S. Lombardo, and O. Telem, “Continuum Naturalness,” *JHEP* **03** (2019) 142, [arXiv:1811.06019 \[hep-ph\]](#).
- [35] E. Megías and M. Quirós, “Gapped Continuum Kaluza-Klein spectrum,” *JHEP* **08** (2019) 166, [arXiv:1905.07364 \[hep-ph\]](#).
- [36] E. Megías and M. Quirós, “The Continuum Linear Dilaton,” [arXiv:2104.10260 \[hep-ph\]](#).
- [37] E. H. Fradkin, *Field Theories of Condensed Matter Physics*, vol. 82. Cambridge Univ. Press, Cambridge, UK, 2, 2013.
- [38] S. Sachdev, “Quantum phase transitions,” *Handbook of Magnetism and Advanced Magnetic Materials* (2007) .
- [39] B. M. McCoy and T. T. Wu, “Two-dimensional Ising Field Theory in a Magnetic Field: Breakup of the Cut in the Two Point Function,” *Phys. Rev. D* **18** (1978) 1259.
- [40] B. M. McCoy and T. T. Wu, “INDETERMINATE MASS PARTICLES,” *Phys. Rept.* **49** (1979) 193–197.
- [41] T. T. Wu, “Two-Dimensional Yang-Mills Theory in the Leading $1/N$ Expansion,” *Phys. Lett. B* **71** (1977) 142–144.
- [42] A. Luther, “Eigenvalue spectrum of interacting massive fermions in one-dimension,” *Phys. Rev. B* **14** (1976) 2153–2159.
- [43] C. Csáki, S. Hong, G. Kurup, S. J. Lee, M. Perelstein, and W. Xue, “Z-portal Continuum Dark Matter.” to appear.
- [44] X.-L. Chen and M. Kamionkowski, “Particle decays during the cosmic dark ages,” *Phys. Rev. D* **70** (2004) 043502, [arXiv:astro-ph/0310473](#).
- [45] E. Pierpaoli, “Decaying particles and the reionization history of the universe,” *Phys. Rev. Lett.* **92** (2004) 031301, [arXiv:astro-ph/0310375](#).
- [46] T. R. Slatyer, “Energy Injection And Absorption In The Cosmic Dark Ages,” *Phys. Rev. D* **87** no. 12, (2013) 123513, [arXiv:1211.0283 \[astro-ph.CO\]](#).
- [47] T. R. Slatyer, “Indirect dark matter signatures in the cosmic dark ages. I. Generalizing the bound on s-wave dark matter annihilation from Planck results,” *Phys. Rev. D* **93** no. 2, (2016) 023527, [arXiv:1506.03811 \[hep-ph\]](#).
- [48] O. W. Greenberg, “Generalized Free Fields and Models of Local Field Theory,” *Annals Phys.* **16** (1961) 158–176.

- [49] A. Dymarsky, K. Farnsworth, Z. Komargodski, M. A. Luty, and V. Prilepina, “Scale Invariance, Conformality, and Generalized Free Fields,” *JHEP* **02** (2016) 099, [arXiv:1402.6322 \[hep-th\]](#).
- [50] E. W. Kolb and M. S. Turner, *The Early Universe*, vol. 69. 1990.
- [51] **Particle Data Group** Collaboration, P. Zyla *et al.*, “Review of Particle Physics,” *PTEP* **2020** no. 8, (2020) 083C01.
- [52] L. Randall and R. Sundrum, “A Large mass hierarchy from a small extra dimension,” *Phys. Rev. Lett.* **83** (1999) 3370–3373, [arXiv:hep-ph/9905221 \[hep-ph\]](#).
- [53] J. W. York, Jr., “Role of conformal three geometry in the dynamics of gravitation,” *Phys. Rev. Lett.* **28** (1972) 1082–1085.
- [54] G. W. Gibbons and S. W. Hawking, “Action Integrals and Partition Functions in Quantum Gravity,” *Phys. Rev. D* **15** (1977) 2752–2756.
- [55] O. DeWolfe, D. Z. Freedman, S. S. Gubser, and A. Karch, “Modeling the fifth-dimension with scalars and gravity,” *Phys. Rev. D* **62** (2000) 046008, [arXiv:hep-th/9909134 \[hep-th\]](#).
- [56] C. Csaki, J. Erlich, C. Grojean, and T. J. Hollowood, “General properties of the selftuning domain wall approach to the cosmological constant problem,” *Nucl. Phys. B* **584** (2000) 359–386, [arXiv:hep-th/0004133 \[hep-th\]](#).
- [57] R. Barbieri, A. Pomarol, and R. Rattazzi, “Weakly coupled Higgsless theories and precision electroweak tests,” *Phys. Lett. B* **591** (2004) 141–149, [arXiv:hep-ph/0310285 \[hep-ph\]](#).
- [58] K. Agashe, C. Csaki, C. Grojean, and M. Reece, “The S-parameter in holographic technicolor models,” *JHEP* **12** (2007) 003, [arXiv:0704.1821 \[hep-ph\]](#).
- [59] J. M. Maldacena, “The Large N limit of superconformal field theories and supergravity,” *Adv. Theor. Math. Phys.* **2** (1998) 231–252, [arXiv:hep-th/9711200](#).
- [60] E. Witten, “Anti-de Sitter space and holography,” *Adv. Theor. Math. Phys.* **2** (1998) 253–291, [arXiv:hep-th/9802150](#).
- [61] S. S. Gubser, I. R. Klebanov, and A. M. Polyakov, “Gauge theory correlators from noncritical string theory,” *Phys. Lett. B* **428** (1998) 105–114, [arXiv:hep-th/9802109](#).